


**CuWO₄ as a Photoanode for Solar-Driven Water Oxidation toward Sustainable
Hydrogen Production**

Josh Kurtz

April 22nd, 2014

This thesis has been read and approved by Bart M. Bartlett

Signed :  Date: 4 / 21 / 2014

Faculty advisor e-mail: bartmb@umich.edu phone: (734) 615-9279

Table of Contents

Abstract	Pg 3
Introduction	Pg 4
Materials and Methods	Pg 20
Results	Pg 26
Discussion	Pg 48
Conclusion	Pg 53
Acknowledgements	Pg 56
References	Pg 57

Abstract

Herein, we present three different synthetic techniques for CuWO_4 electrodes towards solar-driven water-splitting – electrodeposition, sol-gel spin-coating, and spray pyrolysis. In addition, we have prepared the $\text{Zn}_{1-x}\text{Cu}_x\text{WO}_4$ series ($0 \leq x \leq 1$) by solid state and co-precipitation. CuWO_4 prepared by electrodeposition shows substantially improved stability upon illumination in neutral water compared to WO_3 . Electrodes prepared by sol-gel spin-casting are not as stable but do selectively oxidize water over chloride ion present, in contrast to WO_3 . CuWO_4 - WO_3 composite electrodes synthesized by electrodeposition are able to oxidize water with no applied electrical bias under 1-sun illumination with a 0.0065% conversion efficiency in the presence of the redox mediator, $\text{K}_3\text{Fe}(\text{CN})_6$.

CuWO_4 electrodes prepared by sol-gel spin coating show increased stability in a pH 7 potassium borate buffer compared to a pH 7 potassium phosphate buffer, as well as photoelectrochemistry that is comparable to those of the CuWO_4 electrodes prepared by electrodeposition. CuWO_4 photoanodes synthesized by spray pyrolysis have been used to optimize film thickness. Films that are <100 nm thick show the best incident-photon to current efficiency (IPCE) measurements; the IPCE is 7% at 400 nm.

Finally, a $\text{Zn}_{1-x}\text{Cu}_x\text{WO}_4$ solid-solution was prepared to evaluate the role of zinc substitution on the optical, magnetic, and photocatalytic properties of first-row transition metal tungstates. The prepared $\text{Zn}_{1-x}\text{Cu}_x\text{WO}_4$ series shows a smooth transition from ZnWO_4 to CuWO_4 as evidenced by both XRD and magnetic susceptibility data, which shows a distinct paramagnetic ordering above various Neel temperatures for $x=0.8, 0.9, \text{ and } 1$.

Introduction

In the 21st century, one of the most important problems facing humanity is developing an enduring, sustainable energy economy. In 2012, the worldwide energy consumption was 5.25×10^{20} J.¹ Given a projected increase in population of 0.9% per year, despite production of more efficient technology, the worldwide energy demand is expected to double by the year 2050 and triple by the year 2100. Energetically speaking, the current carbon-based energy sources can easily meet this energy demand. There are approximately 40-80 years worth of energy in known oil reserves, 160 years of natural gas energy and 1000-2000 years of energy produced from coal, shale, and tar sand.²

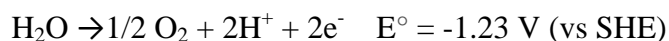
Use of fossil-fuel based energy resources at the current rate of energy consumption, however, will lead to a near doubling of the carbon emissions rate worldwide. The CO₂ concentration in the atmosphere has risen to over 400 ppm, in 2013.³ Within the next century, this number is expected to double. As a result, the global temperature is predicted to increase at a rate of 0.2 °C per decade. An increase in global temperature of only 1-5°C may result any in the following: increased drought in mid-latitudes and semi-arid mid-latitudes, hundreds of millions of people exposed to increased water stress, increasing wildfire risk, increased damage from floods and storms, and increased morbidity and mortality from heat waves, floods, and droughts.⁴ Carbon-based fuel sources will not only eventually be depleted, but in the process are likely to have extreme ecological consequences.

This trend then strongly suggests the need for a carbon-neutral source of energy in order to avoid potentially catastrophic side effects of increasing carbon emissions. Although other carbon-neutral energy sources such as nuclear fission and carbon capture and storage will prevent CO₂ emission into the atmosphere, the only practical and sustainable carbon-neutral energy sources are solar power, wind power, and biofuel. Additionally, considering the fact that nearly as much energy from the sun hits the earth's surface in one hour (4.3×10^{20} J) as was consumed globally in 2013 ($5.25 \times$

10^{20} J), renewable energy from the sun contains the largest energy reserve in comparison with other alternative energy sources.

The challenge with using solar energy is making its conversion to electric energy cost-effective in comparison with current carbon-based fuel sources. For example, while current carbon-based fuel costs about \$0.02-\$0.05 per kW-hr, the present-day Si-based solar appliances cost approximately \$0.35 per kW-hr, nearly 10 times the cost of the carbon-based fuel. The present cheapest method for solar energy conversion and storage is solar thermal energy. Its current cost, \$0.10-\$0.15 per kW-hr is only approximately 3-5 times more expensive than using carbon-based fuels.⁵

Another promising route of solar energy conversion comes from taking a page out of nature's book and mimicking photosynthesis to store energy as fuel. During photosynthesis in plants, energy from the sun is used to oxidize H_2O and reduce NADP^+ producing O_2 and reducing equivalents of NADPH as shown in the two half-reactions below:

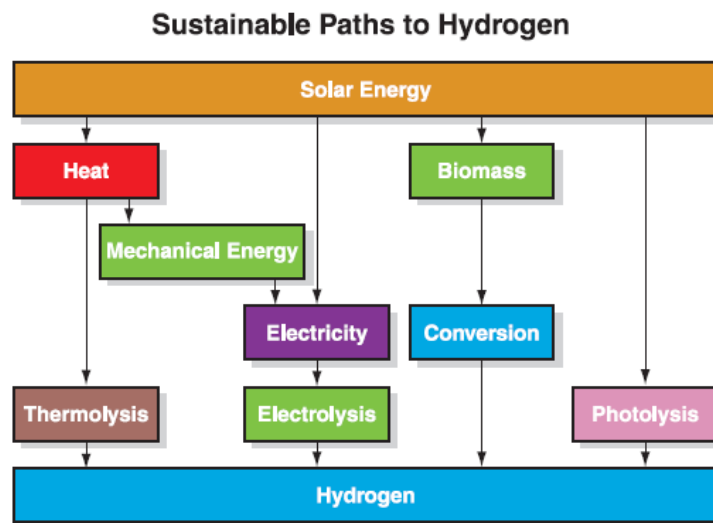


This gives a $\Delta E^\circ = -1.139 \text{ V}$ and using the Nernst equation, a $\Delta G^\circ = +219.8 \text{ kJ/mol H}_2\text{O}$. Because H_2O is a clear liquid, it is unable to absorb visible, light which makes up a significant portion of the solar spectrum. As a result, photosystem II must absorb visible-light to supply the required energy needed to activate the catalyst used in driving this reaction. The oxygen-evolving complex in plants that catalyzes this reaction is a manganese-based metal oxide molecular cluster that uses the sun's energy to overcome this energetically unfavorable reaction.⁶

The concept is then to create a compound that, similar to the OEC in plants, absorbs sunlight and stores the energy in the form of H_2 fuel. H_2 can be created at the site of interest. Notable is that the

conversion of H_2 into electrical energy by a fuel cell, produces only H_2O as a byproduct. This makes it significantly more attractive as fuel source because it will significantly decrease the rate at which CO_2 is released into the atmosphere. H_2 may also be used to generate carbon-based fuels using atmospheric CO_2 , which gives another readily accessible and more eco-friendly source of these fuels.

The current large-scale production of H_2 gas comes predominantly from steam reformation of natural gas followed by the water-gas shift reaction, which as a result releases 9 Mtons /year of CO_2 into the atmosphere. Wind energy coupled with the electrolysis of water provides one alternative carbon-neutral route to H_2 production, but the currently available systems are very expensive. Alternative methods for H_2 production from solar energy are shown in figure 1 below.



⁵Figure 1: Potential Routes for Sustainable Hydrogen Production

The splitting of water using solar-derived heat energy or thermolysis is impractical. At the high temperatures necessary for water splitting, the back reaction from the H_2 and O_2 produced to re-form water is rapid. Although conversion of biomass to H_2 using solar energy is debatably the most cost-effective method of solar energy conversion to date, it suffers from a very low efficiency, which is necessary for use on a large scale. A promising route for using solar energy to produce hydrogen gas is the direct photolysis of water. In this system, solar energy is directly coupled to the oxidation of water

and H₂ and O₂ can be produced by the same device used to collect the energy. Photolysis of water can be achieved through the use of semi-conductor photocatalysts that are able to absorb the light emitted by the sun and use it to catalyze the oxidation of water.

The first record of a photoelectrochemical experiment was published in 1839 by a French physicist, Edmund Becquerel. He observed a voltage generated upon shining light on a thin film of silver chloride in water connected to a counter electrode.⁷ For solid materials, this effect was first observed on selenium by Willoughby Smith in 1873.⁸ It wasn't until nearly a century later that this method was applied to the solar-driven splitting of water. In 1972, Akira Fujishima and Kenichi Honda were the first to report the production of electrical current when TiO₂ was connected to a platinum electrode and ultraviolet light was shined on the TiO₂ surface.⁹ Since then, researchers have focused on using TiO₂ and a wide variety of other metal oxide materials to split water using sunlight.

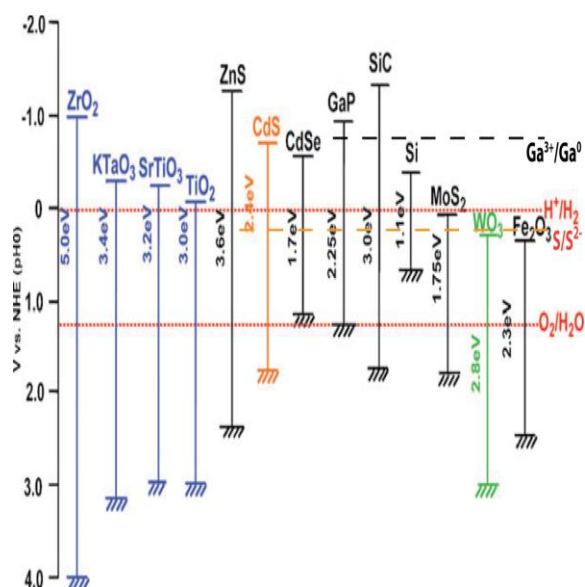
In order to understand how the process of water splitting works, one must be familiar with three terms: valence band, conduction band, and band gap. The valence band is composed of the highest occupied crystal orbitals containing valence electrons while the conduction band is composed of the lowest unoccupied crystal orbitals. The difference in energy between these two bands is referred to as the band gap. A smaller energy band gap corresponds to longer wavelengths (λ) of light needed to excite an electron from the valence band to the conduction band, according to the Einstein's relationship: $E=hc/\lambda$, where h is Planck's constant and c is the speed of light.

Further, band gaps are separated into two types: direct and indirect. Direct band gaps are characterized by crystal vectors in the conduction and valence band that are the same, while indirect band gaps have vectors that are different. This allows direct band gap materials to directly absorb a photon, while indirect materials must transfer momentum to the crystal lattice before being absorbed. This then has implications for absorbance and thickness of the light-absorbing material. For indirect band gap materials, light penetrates further into the film surface before being absorbed and so film

thickness may play a significant role in overall electrode performance. Direct band gap materials are typically good at absorbing light and so thickness does not play a significant role in absorption.

The challenge in finding suitable materials for water-splitting photocatalysis is that the energy requirements are exceedingly stringent. One of the first requirements for water-splitting is that the band gap should be close to 2 eV, to provide sufficient energy to split water including kinetic overpotential considerations. Secondly, the band edges must be appropriately placed relative to the redox potentials of the half reactions for water splitting. Third, charge-carrier generation and migration must be rapid relative to recombination in the bulk. Lastly, the material must be chemically stable in the presence of reactive oxygen species that are generated during the reaction.

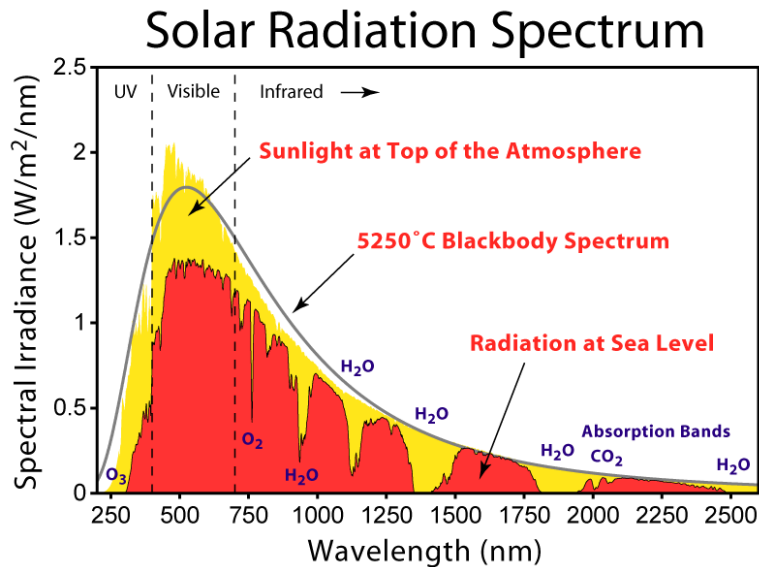
Certain semi-conductors fulfill many of the requirements for water splitting, such as CdS, which has properly placed band edges and is able to use a significant portion of the solar spectrum (2.4 eV band gap), as can be seen in figure 2.



¹⁰Figure 2: Band Edges and Band Gap Energies of Select Water Oxidation Catalysts

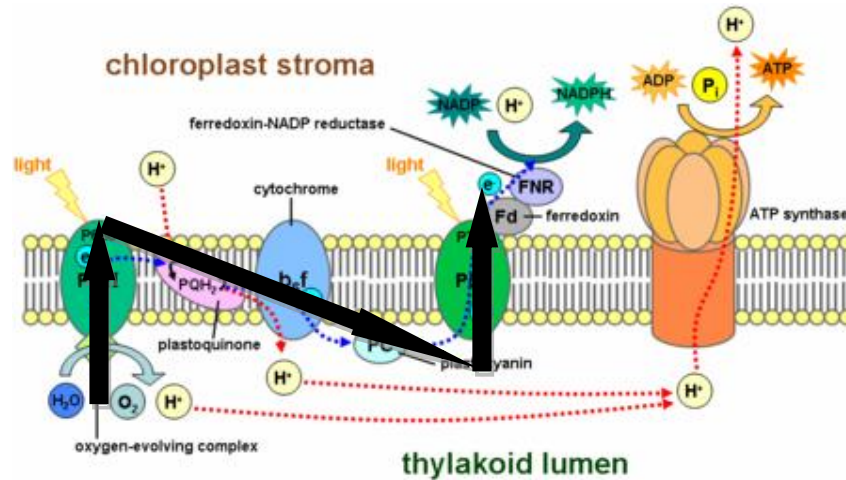
Unfortunately, under the strongly oxidizing conditions of water-splitting, S²⁻ is oxidized to S⁰ or SO₄²⁻, depending on the pH, causing the electrode to degrade. For this reason, compounds that are resistant to oxidation, such as metal oxides, are required for stability. Although some metal oxides have properly

located band positions to perform both half reactions, such as TiO_2 , their bands gaps are so large that the materials are unresponsive to visible light.³ Examining the solar spectrum illustrated in figure 3, we see that the portion of UV radiation that the sun emits is minimal ($\approx 5\%$) compared to that in the visible region ($\approx 50\%$). As such, the known oxide semiconductors that have band gaps large enough to directly split water suffer from poor solar-to-hydrogen efficiency.



¹¹Figure 3: Solar Spectrum Output by Wavelength

In order to overcome this inefficiency, a possible approach involves separating the two water-splitting half reactions. This is similar to how water splitting is accomplished in nature. Because the two half-reactions are performed separately, there are two unique complexes that absorb different wavelengths of light, known as P680 or photosystem II and P700 or photosystem I, as seen in figure 4.



¹²Figure 4: Z-Scheme Water-Splitting in Photosynthesis

In the case of photosynthesis, water is oxidized at photosystem II to form O_2 and H^+ . The excited electrons from water then travel downhill in energy through redox mediators and the electron is excited again with solar energy at photosystem I, where it is used to reduce $NADP^+$ to $NADPH$. This process by which an electron is excited in energy, moves downhill in energy and is excited again is known as a Z-scheme for its resemblance to the letter. By optimizing each half reaction, the Z-scheme approach lowers the kinetic barrier associated with overall water splitting.

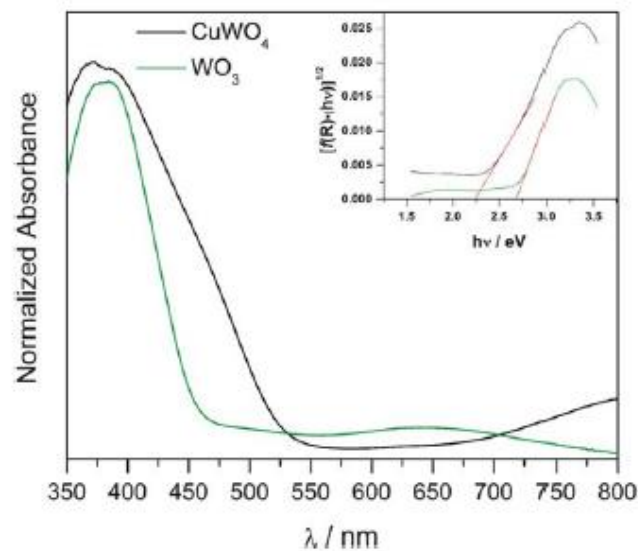
This strategy can be adapted for metal oxide electrodes. When discussing electrodes, oxidation occurs at the anode and reduction occurs at the cathode. On a metal oxide photoanode, O_2 is evolved, and electrons are shuttled through a redox mediator with an appropriate reduction potential to the photocathode. Unlike photosynthesis, the end goal is the production of H_2 gas and so protons are reduced directly at the cathode. The overall efficiency of water-splitting may similarly be increased due to the wider range of visible light absorbance values of both the cathode and anode in contrast to the one electrode system.

Towards this Z-scheme, one potential metal oxide semiconductor with a valence band edge sufficiently positive for O_2 production but with a conduction band edge insufficiently negative for H^+ reduction is WO_3 . WO_3 was first studied in the late 1970s¹³ and since that time, there have been

numerous publications involving WO_3 as a photoanode for solar-driven water oxidation.

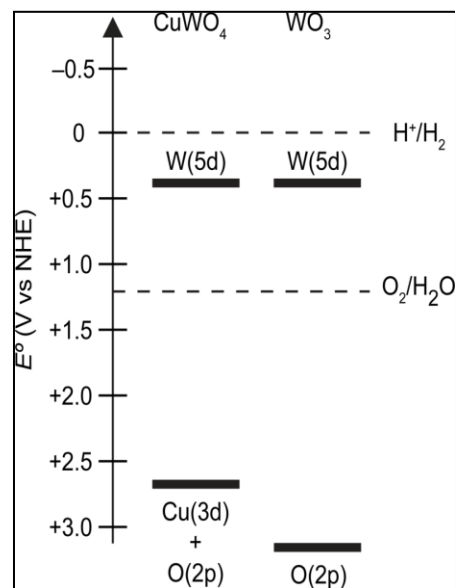
Unfortunately, WO_3 has a few inherent flaws that limit its ability to perform optimally as a photocatalyst for water oxidation: a large band gap, which limits the amount of visible light absorbed, and instability under neutral or basic conditions, which has serious implications for large-scale synthesis using primarily neutral water.

In order to overcome these inherent inefficiencies of WO_3 , one possible solution is to create first row transition-metal tungstate compounds. Of particular interest is CuWO_4 which was originally studied in 1990¹⁴ by Arora et al. on single crystals and a similar report by the same group 15 years later in 2005¹⁵. Since then, Yourey et al., have reported a synthesis for CuWO_4 thin electrodes on a fluorinated tin oxide (FTO) conductive substrate¹⁶, which has shown a few notable benefits over WO_3 . First, CuWO_4 has a smaller band gap compared to WO_3 , having been reported around 2.25 eV in contrast to WO_3 's band gap of 2.7 eV. CuWO_4 's larger band gap results in a bathochromic shift in wavelength (a shift to longer wavelengths) in its absorption spectrum compared to WO_3 , as can be seen in figure 5.



¹⁶Figure 5: Normalized Absorption Spectrum of CuWO_4 and WO_3

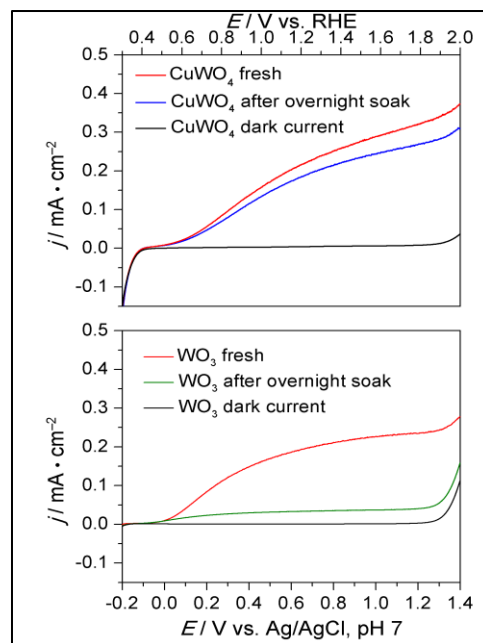
This correlates well to the yellow color of the CuWO_4 electrodes, which absorb more light in the visible region, in contrast to the white color of WO_3 electrodes, which absorb more toward the ultraviolet region of the solar spectrum. This is advantageous because as mentioned previously the sun puts out a significantly larger proportion of visible light compared to ultraviolet light, allowing CuWO_4 to use more of the light that the sun puts out, potentially increasing overall efficiency. The smaller band gap is hypothesized to be caused by the orbital mixing of the $\text{Cu}(3d)$ and $\text{O}(2p)$ atomic orbitals that comprise the valence band, resulting in an increased valence band maximum.¹⁷ UV-Vis spectroscopy and Mott-Schottky analysis, which is used to approximate the conduction band edge position, have shown that this smaller band gap is in fact the result of an increased valence band maximum, as shown in figure 6.



¹⁷Figure 6: Estimated Band Edge Positions for CuWO_4 and WO_3

A second major improvement in CuWO_4 electrodes compared to WO_3 electrodes is their increased stability at neutral pH solutions. In order to be applied to a large-scale practical system, the photocatalyst selected for solar-driven water oxidation should be stable at the pH of seawater, which is approximately 8. Yourey et al. have shown that that CuWO_4 electrodes prepared by electrodeposition

have significantly increased stability as measured by linear sweep voltammetry after an overnight soak in pH 7, 0.1 M potassium phosphate buffer (see figure 7). Although WO_3 electrodes show significantly improved photocurrent in comparison to CuWO_4 electrodes under acidic conditions, the photoelectrochemical performance is poor at neutral pH. Therefore, unmodified WO_3 electrodes are not suitable for use as water oxidation catalysts on an industrial scale. With great stability at neutral pH, CuWO_4 shows greater promise as a photocatalyst for solar-driven water oxidation if increases in efficiency can be made through synthetic modification, controlling morphology, or co-catalyst loading.



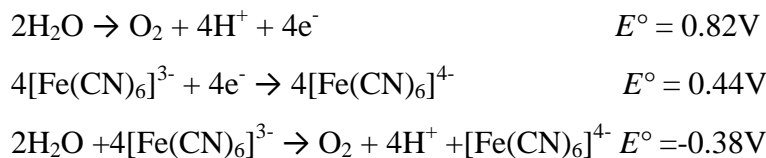
¹⁶Figure 7: Relative Stability of CuWO_4 and WO_3 in 0.1 M KP_i at $\text{pH}=7$

One additional drawback of WO_3 was discovered by Mi et al. recently when they reported that in the presence of chloride ions, WO_3 preferentially oxidizes the chloride forming Cl_2 gas in place of oxidizing water.¹⁸ Given the fact that the significant majority of the earth's water is seawater, containing sodium chloride, it may not be practical to use WO_3 as the photoanode for solar-driven water oxidation. My work begins by showing a facile synthesis for CuWO_4 - WO_3 electrodes by electrodeposition which perform solar-driven water oxidation with no applied bias.

The direct photolysis of water is relatively inefficient, with biological photosynthetic systems only performing at a 0.05% overall efficiency. Inorganic semi-conductor mimics of these biological systems are not surprisingly relatively inefficient. As a result of both the overall thermodynamically unfavorable reaction and the large kinetic barrier involved in water splitting, large amounts of energy are needed to drive this reaction.

In order to increase the efficiency of conversion of solar energy into useful chemical energy, a Z-scheme approach may be used as mentioned above. The benefits of this Z-scheme approach are two-fold. First and foremost, with two different light absorbing centers, the conduction band edge may be more positive than 0 V vs SHE, allowing for smaller photoanode band gaps and greater visible light absorption. Additionally, with the photocathode being separate from the photoanode, different wavelengths of light can be absorbed for increased efficiency. Second, by using a redox mediator to transfer the electrons between the photoanode and photocathode, each half-reaction may become more favorable, decreasing the energy requirement for each individual step.

Towards the second aim, a redox mediator must be chosen that possesses E° at more positive potential than the conduction band of the photoanode and more negative than the valence band of the photocathode. One such redox mediator that we have shown to pair well with CuWO_4 photoanodes is $\text{K}_3\text{Fe}(\text{CN})_6$. The reported half reactions for this Z-scheme can be described by the following:



What is important to note here is that the overall $E^\circ = -0.38\text{ V}$ using $[\text{Fe}(\text{CN})_6]^{3-}$ compared to a $E^\circ = -1.23\text{ V}$ for overall water-splitting with H^+ as the electron acceptor. With this decreased overall energy requirement, we have shown that water can be oxidized using $\text{CuWO}_4\text{-WO}_3$ composite electrodes as the photoanode with only sunlight (the reaction is still spontaneous and requires an input) at pH 7. As

seen in Figure 8, the overall reaction scheme would allow for the oxidation of water at the photoanode followed by the reduction of the redox mediator with its reduction potential being more positive than that of the conduction band edge of the composite electrodes. Eventually the electron in the redox mediator would be excited in energy again using a photocathode, which would then use the high energy electrons to reduce protons to hydrogen gas.

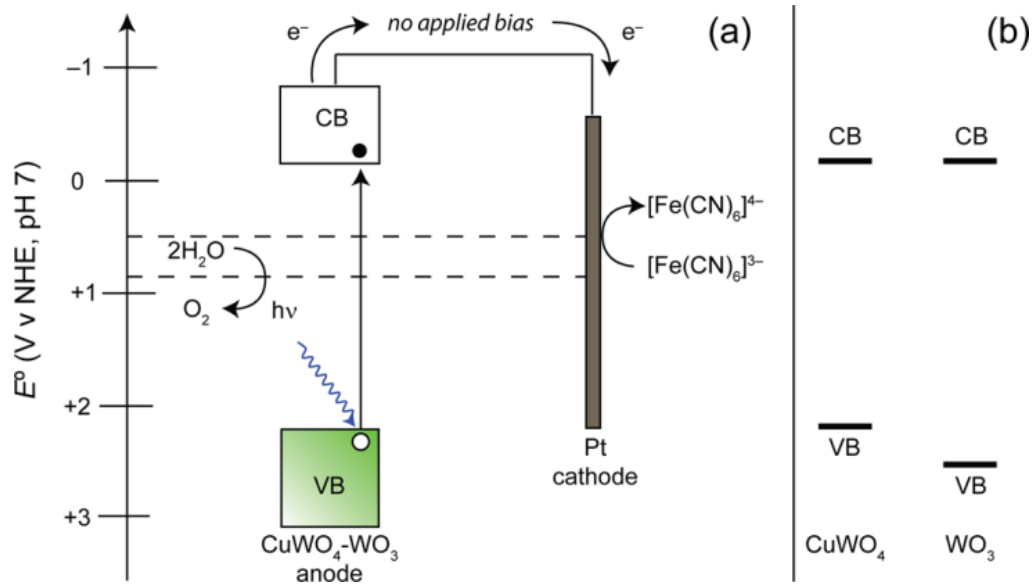


Figure 8: (a) Band structure of $\text{CuWO}_4\text{-WO}_3$ composite electrodes superimposed with the chemical potentials for water oxidation and ferricyanide reduction at pH 7; (b) measured band edges of 1.2:1 W:Cu and for pure WO_3 for comparison purposes.

Although work with $\text{CuWO}_4\text{-WO}_3$ electrodes may be useful in showing that these electrodes are able to photooxidize water with no applied bias, it also reveals an inherent flaw in the synthetic method – controlling the Cu to W ratio via electrodeposition is difficult, thus making it difficult to synthesize pure CuWO_4 electrodes via this route. Towards solving this problem we began to consider other synthetic methods for the preparation of CuWO_4 . Some work has already been done towards this aim by Chang et al. who have produced CuWO_4 electrodes via cosputtering as well as multiwalled carbon nanotube – copper tungstate composite electrodes via spray deposition.^{19, 20} Additionally, Zheng

et al. synthesized an electrode consisting of a p-CuO-n-CuWO₄ junction, while Pilli et al have created BiVO₄-CuWO₄ heterojunction electrodes.^{21, 22}

There are many factors that contribute to an electrode's ability to oxidize water – including phase, crystallinity, and morphology – all of which are influenced by the synthetic method as well as the choice of electrolyte and buffer used for the photolysis. Although the purpose of the buffer is to resist the pH change that would be driven by liberating protons during the anodic half reaction, it is important to consider any potential side reactions that may occur between water and the counterion of the buffer. Ideally, the electrode should be stable at near neutral pHs with high salt concentration for wide scale adoption using seawater. It is also important to ensure that any supporting electrolytes are not redox active in the potential window at which water-splitting occurs. It is toward these two aims that we set out to synthesize pure-phase CuWO₄ electrodes using a sol-gel synthesis method. In order to determine if the Cl⁻ is preferentially oxidized to Cl₂ over H₂O as is seen in the case of WO₃, these electrodes were tested in a sodium chloride supporting electrolyte.²³

Noting the distinct differences in the stability and the photoelectrochemical properties in CuWO₄ when it is prepared by electrodeposition and sol-gel processing with spin-casting, we looked to synthesize CuWO₄ by alternate methods to develop morphology-properties relationships. With electrodeposition, it is difficult to control the relative amounts of copper and tungsten that are deposited onto the film surface. As a result, it is difficult to obtain the desired product by this synthetic method. Although with sol-gel spin-casting this problem is solved as starting amounts of the precursors are pre-determined, creating uniform and homogenous films is difficult. Hydrogen bonding interactions in water leads to higher surface tension, and it does not spin-cast especially well and the resulting films are often spotty and non-uniform. For this reason, we turned to spray pyrolysis as a synthetic alternative. Spray pyrolysis also allows for significant control of the stoichiometry and since

the same concentration of solution is sprayed onto a pre-heated substrate, this allows for greater film uniformity.

Because this method is capable of depositing a uniform layer, the film thickness can be easily controlled by increasing the number of sprays onto the substrate electrode. Accordingly, we can optimize electrode thickness to achieve maximum efficiency of the photoanode in the water oxidation reaction. As demonstrated in Figure 9 below optimizing film thickness is an interplay between maximizing the number of photons absorbed and the number of useful electron-hole pairs generated to perform water oxidation. As film thickness increases, with increasing amount of electrode material present, the amount of photon absorption increases as well. However, as film thickness increases, the electron-hole pairs generated from these photons are created further from the electrically conductive substrate where they are able to perform useful chemistry. It is towards this aim that we sought to optimize electrode thickness.

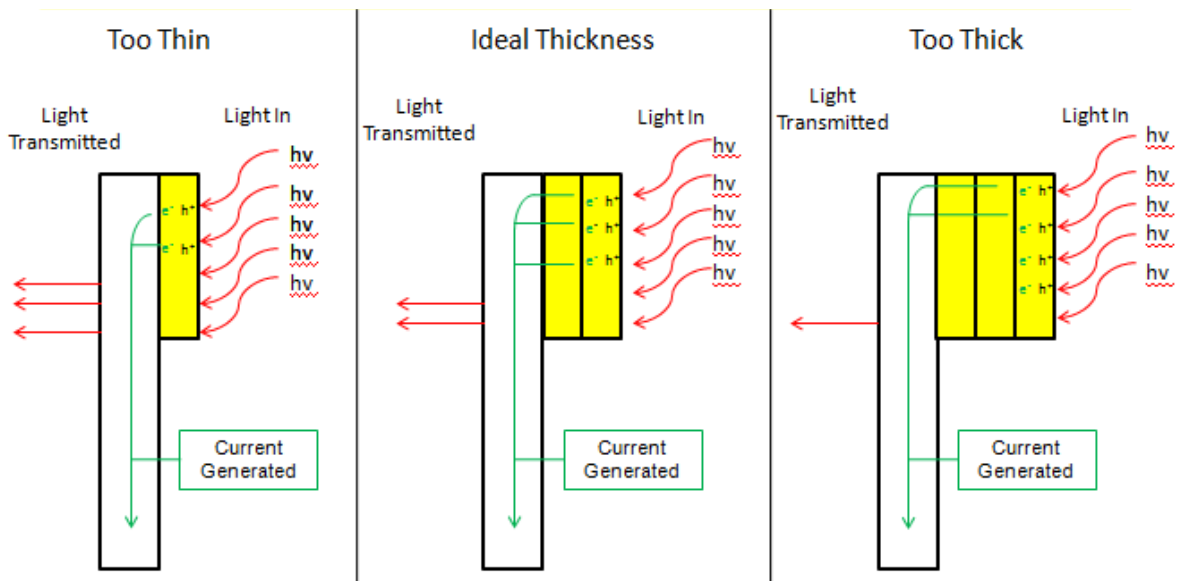


Figure 9: Diagram portraying the balance between photons absorbed and distance of electron-hole pairs created when optimizing film thickness.

In order to interpret the efficiency measurements that are taken for various film thicknesses, we must first understand the conception of penetration depth, which can be described by the equation:

$$\alpha = (1/d)\ln(\%T/100)$$

where α is the absorptivity coefficient, d is the penetration depth, and $\%T$ is the percent transmittance. Alpha is inversely related to wavelength such that wavelength and penetration depth are directly proportional. This has implications for the location of the electron-hole pair generated, the likelihood of recombination and overall efficiency as will be discussed later.

In contrast to single phase materials like the CuWO_4 electrodes, electrodes consisting of more than one substance forming a solid solution may show a distinct advantage. Although the CuWO_4 - WO_3 electrodes we synthesized were able to perform water oxidation with only sunlight in the presence of $\text{K}_3\text{Fe}(\text{CN})_6$, with two phases there are some potential charge transfer limitations. With two distinct phases, it is highly likely that charge transfer will be kinetically limiting between these interfaces, which may lead to greater recombination. This could help to explain why the overall quantum yield of this reaction was found to be 0.04%. It is for this reason that we decided to turn to single phases consisting of mixed metals to more effectively study photoelectrochemistry.

Specifically, we turned our attention to synthesizing the $\text{Zn}_{1-x}\text{Cu}_x\text{WO}_4$ series by both solid state synthesis and a sol-gel synthesis. All of the first row transition metal tungstates crystallize in the wolframite structure which makes the synthesis of this series feasible in the form of a solid solution. One important difference to note is that ZnWO_4 crystallizes into the $P2/c$ space group and is a direct band gap material of 3.4 eV^{24} . In contrast, CuWO_4 exhibits Jahn-Teller distortion due to the $d^9 \text{ Cu}^{2+}$ to $P - 1$ and is an indirect band gap material. In order to confirm the presence of the solid solution of the $\text{Zn}_{1-x}\text{Cu}_x\text{WO}_4$ series rather than a two phase mixture of ZnWO_4 and CuWO_4 , we collected magnetic susceptibility data, specifically by looking at ordering temperatures. Additionally, we recorded optical

absorption data to determine how increasing amounts of Cu^{2+} affected the compound's absorbtivity, particularly into the visible region.

Materials and Methods

A. CuWO₄-WO₃ Composite Electrodes Synthesis and Characterization

Photoanodes were prepared by electrodeposition starting from a 30% isopropyl solution of 30 mL of 50 mM H₂W₂O₁₁ with 30 mM Cu(NO₃)₂ · 3H₂O. The final solution was adjusted to a pH of approximately 1.2 by the addition of 20% HNO₃. Amorphous films were deposited on FTO (Pilkington Glass, Tec 1.5, 2.2 mm thick, 12-14 ohms/sq) by sweeping at 10 mV/s from +0.3V to -0.5V vs AgAgCl for 2 cycles at room temperature with a CH Instruments 660C Electrochemical Workstation. The substrate-covered glass was then annealed in air for 6 hours at 500C using an MTI box furnace with a heating and cooling rate of 2C/min. Finally, after cooling the films were trimmed to 1.1 by 2 cm² piece and copper wire was attached to make electrical contact using silver paint. The wire was sealed off using Hysol IC epoxy.

In order to characterize the materials, X-ray diffraction patterns were recorded using a Bruker D8 Advance diffractometer with a graphite monochromator, a Lynx-Eye detector, and parallel beam optics using Cu K_α radiation of wavelength 1.54184 Å. A step size of 0.04°/step with a scan rate of 0.5 s/step and both CuWO₄ and WO₃ were identified using MDI Jade version 5.0. UV-Vis spectra were taken using a Cary 5000 spectrophotometer (Agilent) with an external diffuse accessory. The data from these spectra were measured in reflectance and converted into absorbance mathematically with Tauc plots then being generated using the Kubelka-Munk function, $F(R) = (1-R)^2/2R$. Lastly, a Hitachi S-32000N SEM was used to collect scanning electron microscopy images at an accelerating voltage of 15 kV. EDX spectra were collected using this SEM in conjunction with a back-scattering electron detector and a working distance of 15 mm using the Cu, K, W, and L emission lines.

All photoelectrochemistry experiments were conducted using a CH Instruments 660C Electrochemical Workstation and custom-built single- or double-compartment cell. The working electrode was the CuWO₄-WO₃ composite electrode, the counter-electrode was the Pt electrode, and

the reference electrode was a Ag/AgCl system. A pH 7 Potassium Phosphate, KP_i , buffer was used for all photoelectrochemical experiments which was purged with N_2 gas to remove any dissolved oxygen. A Newport-Oriel 150 W Xe arc lamp fitted with an AM 1.5G filter was used as a light source. In order to mimic the power of the sun, the lamp was adjusted to 100 mW using a Newport optical power meter with a thermopile detector.

The custom-built two-compartment cell with a fine frit separator was used for oxygen detection experiments. For experiments using $[\text{Fe}(\text{CN})_6]^{3-}$ as the sacrificial reductant without an applied electrical bias, a single-compartment cell was used including a $\text{CuWO}_4\text{-WO}_3$ composite working electrode, Pt counter-electrode, and a FOSSPOR fluorescence probe. Solutions were stirred vigorously in order to disperse the redox mediator and help O_2 dissociation from the working electrode surface. This cell contained 20 mL of the KP_i electrolyte and 19 mL of head space. The number of moles were calculated using the ideal gas law, using the temperature recorded by the NeoFox temperature probe, partial pressure of O_2 recorded from the FOSSPOR fluorescence probe (dissolved O_2 was accounted for using Henry's Law), and the head space volume.

B. CuWO_4 Sol-Gel Electrodes Synthesis and Characterization

The CuWO_4 sol gel solution which was used to spin coat onto the previously sonicated fluorinated tin oxide (FTO), purchased from Pilkington Glass (Tec 15, 2.2 mm thick, 12-14 ohms/square) was produced by dissolving 1 mmol of $\text{Cu}(\text{NO})_2 \cdot 3\text{H}_2\text{O}$ in 1.2 mL of ethylene glycol using a 20-mL scintillation vial. Next, 1 mmol of tungsten was added as ammonium metatungstate, $(\text{NH}_4)_6\text{H}_2\text{W}_{12}\text{O}_{40} \cdot 4\text{H}_2\text{O}$ along with 0.1 mL of water. This mixture was then stirred and sonicated, allowing the solid AMT to dissolve. Finally, 0.025 mg of Triton-X 100 was added to the solution to assist with more uniform solution dispersion upon spinning. The solution was then heated at 95°C in an oil bath for approximately 2.5-4 hours until the solution became dark green. 25 μL of this solution

was then spun onto a 1 cm^2 surface of FTO for 10 minutes at 1200 rpm followed by a 3 second spin at 2000 rpm using a Laurell spin coater (model WS-400B06NNP/LITE). These electrodes were then annealed at 550°C for 1 hour with a cool and ramp time of 1 hour. These electrodes were then connected to a piece of copper wire using silver print II from GC Electronics and sealed using Hysol IC epoxy at the end of a piece of glass tubing.

In order to characterize the materials, X-ray diffraction (XRD) patterns, UV-Vis spectra, scanning electron microscopy images, and inductively coupled plasma atomic emission spectroscopy (ICP-AES) elemental analysis were all used. Specifically, XRD patterns were recorded using a Bruker D8 Advance diffractometer with a graphite monochromator, Lynx0Eye detector and parallel beam optics using $\text{Cu K}\alpha$ radiation ($\lambda = 1.54184 \text{ \AA}$) and collected using a 0.6 mm incidence slit with a 0.04 degree/step step size and 1 sec/step scan rate. MDI Jade version 5.0 was used to compare the pattern to the CuWO_4 compound using JCPDF 72-0616. The UV-Vis spectra were recorded using a Cary 5000 spectrophotometer from Agilent including an external diffuse reflectance accessory. Tauc plots were created by transforming the reflectance data using the Kubelka-Munk function. The SEM images were collected with an FEI Nova Nanolab SEM/focused ion beam instrument using an accelerating voltage of 15 kV. EDX analysis spectra were also collected using a Hitachi S-3200N SEM with an accelerating voltage of 25 kV and a working distance of 15 mm. Spectra were quantified using EDAX genesis software with the Cu, K, W, and L emission lines. Lastly ICP-AES was conducted using a Perkin-Elmer Optima 2000DV instrument and using the CuWO_4 material from four separate films. These films were dissolved in a solution of 30% H_2O_2 , 1 mL of HNO_3 , and 2 mL of water which was heated to 80°C . After cooling, additional water was added to make a final volume of 10 mL and the 324.752 (Cu) and 224.876 (W) nm emission lines were used.

Photoelectrochemistry was performed with a CH Instruments 660 C electrochemical workstation all measurements were measured in a custom-made glass cell with a quartz viewing

window. For three-electrode experiments, a Ag/AgCl reference electrode and a Pt counter electrode were used, and the supporting electrolyte was either pH 3, 5, or 7 0.1 M KPi or pH 7 KBi . The light source was a Newport-Oriel 150W Xe arc lamp fitted with an AM 1.5G filter from Newport. The lamp power was set to 100 mW/cm^2 using a Newport optical power meter with a thermopile detector. Lastly, for oxygen evolution experiments, a FOSSPOR fluorescence probe from Ocean Optics was used and the amount of oxygen produced was calculated using the ideal gas law and accounted for dissolved O_2 using Henry's Law.

C. CuWO_4 Prepared by Spray Pyrolysis Synthesis and Characterization

All materials were purchased from Sigma-Aldrich and used as received. In order to prepare the precursor solution for spray pyrolysis, a 0.2 M stock solution of CuCl_2 and ammonium meta-tungstate were prepared by dissolving the appropriate amount of each solid in 200 mL of Millipore-filtered water. 5 mL of each of these solutions were added to a 100-mL volumetric flask and diluted to a total volume of 100 mL with water. The FTO substrate purchased from Pilkington Glass (Tec 15, 2.2 mm thick, 12-14 ohms/square) was cleaned by sonication in ethanol, acetone, and water for 10 minutes each.

A custom-made spray pyrolyzer was used to deposit the solution onto the substrate surface, consisting of a glass nozzle connected with plastic tubing to a compressed air valve. This valve was placed 10" above the FTO surface and was set to spray for 1 second intervals followed by a 10 second delay. Prior to spraying the electrode surface, the hot plate was heated to 410°C and the FTO substrate was allowed to sit on the hot plate for 3 minutes in order to reach a temperature of approximately 360°C . A small piece of metal was placed over the electrode surface to expose an approximately 1 cm^2 surface area. The amount of spray time was determined by the number of desired sprays and the previously described spray timing pattern.

In order to characterize the materials, x-ray diffraction (XRD) patterns and UV-Vis spectra were taken. Specifically, XRD patterns were recorded using a Bruker D8 Advance diffractometer with a graphite monochromator, Lynx-Eye detector and parallel beam optics using Cu K α radiation ($\lambda = 1.54184 \text{ \AA}$) and collected using a 0.6 mm incidence slit with a 0.04 degree/step step size and 1 sec/step scan rate. MDI Jade version 5.0 was used to compare the pattern to the CuWO₄ compound using JCPDF 72-0616. The UV-Vis spectra were recorded using a Cary 5000 spectrophotometer from Agilent including an external diffuse reflectance accessory.

Photoelectrochemistry was performed with a CH Instruments 660 C electrochemical workstation all measurements were measured in a custom-made glass cell with a quartz viewing window. For three-electrode experiments, a Ag/AgCl reference electrode and a Pt counter electrode were used, and the supporting electrolyte of pH 7 0.1 M KB_i. The light source was a Newport-Oriel 150W Xe arc lamp fitted with an AM 1.5G filter from Newport. The lamp power was set to 100 mW/cm² using a Newport optical power meter with a thermopile detector.

D. Zn_{1-x}Cu_xWO₄ Solid Solution Synthesis and Characterization

All starting materials were purchased from Sigma Aldrich and used as they were received. Eight mmols of W in the form of WO₃ and either Zn in the form of ZnO Cu in the form of CuO or a mixture of these two compounds were ground using a mortar and pestle and annealed in an alumina crucible at 850°C for 12 hours with 4 hour heating and cooling times. Following this initial annealing step, these powders were reground and heated at 850°C for 36 hours. In order to synthesize the entire Zn_{1-x}Cu_xWO₄ series with x being x=0, 0.1, 0.2, 0.3, 0.4, 0.5, 0.6, 0.7 0.8, 0.9, 1. Certain ratios of this series were also synthesized by a sol-gel Pechini-type method, which was adapted from Galceran et al.²⁵. The ratio of citric acid to earth metals was 1:1 with the citric acid to ethylene glycol ratio was 2:1. The resulting solution was heated at 80-90°C under stirring until water was evaporated, leaving the

dried gel behind, which was subsequently dried in a vacuum oven overnight at 60-70°C. Lastly, this gel was ground with a mortar and pestle and annealed at 700°C for 3 hours with heating and cooling rates of 2 hours.

In order to characterize these compounds, XRD patterns were recorded with a Bruker D8 Advance diffractometer equipped with a graphite monochromator, a Lynx-Eye detector, and parallel beam optics using Cu-K α radiation with a wavelength 1.54184 Å. These patterns were collected with an incidence slit of 0.6 mm and a scan rate of 0.5 s/step and a step size of 0.04°/step. The phases were identified using the previously reported crystal structure as determined by Schofield et al. for this series.²⁶ Absorption spectra were collected using an Agilent-Cary 5000 spectrophotometer with a diffuse reflectance accessory. Barium sulfate was used as the baseline and a 50 mg sample of the compounds was diluted with BaSO₄ and placed on top of BaSO₄ to create a smooth surface. The reflectance data that was collected was converted using the Kubelka-Munk function into Tauc plot data. SEM images were collected using a Hitachi S-3200N scanning electron microscope with an accelerating voltage of 15 kV. ICP-AES data was collected for Cu, Zn, and W using a Perkin-Elmer Optima 2000DV instrument. Lastly, magnetic susceptibility measurements were performed with a Quantum Design MPMS-XL7 with an Evercool Dewar. Approximately 100 mg of each of sample was suspended in 100 mg of eicosane from Sigma Aldrich in a polycarbonate capsule. Using a measuring field of 1 Tesla, the measurements were collected under zero-field cooled conditions in the temperature ranges of 5-300 K. Data were corrected for the diamagnetism using Pascal's constants and susceptibility data were fit to the Curie-Weiss law, $\chi M = C/(T - \Theta)$.

Results

The $\text{CuWO}_4\text{-WO}_3$ films were characterized by XRD and SEM with EDX. The XRD patterns as shown in Figure 10 confirm the presence of both CuWO_4 and WO_3 . Additionally, the EDX spectrum, shown in Figure 11, confirms the presence of a tungsten to copper ratio of approximately 2:1 as expected for the composite mixture.

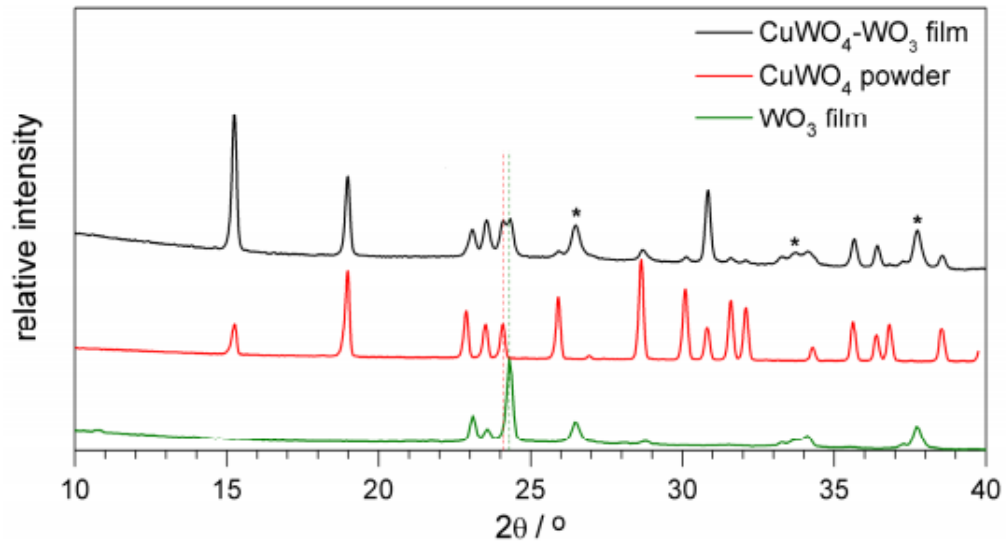


Figure 10: X-ray diffraction pattern of $\text{CuWO}_4\text{-WO}_3$ film, CuWO_4 powder, and WO_3 film

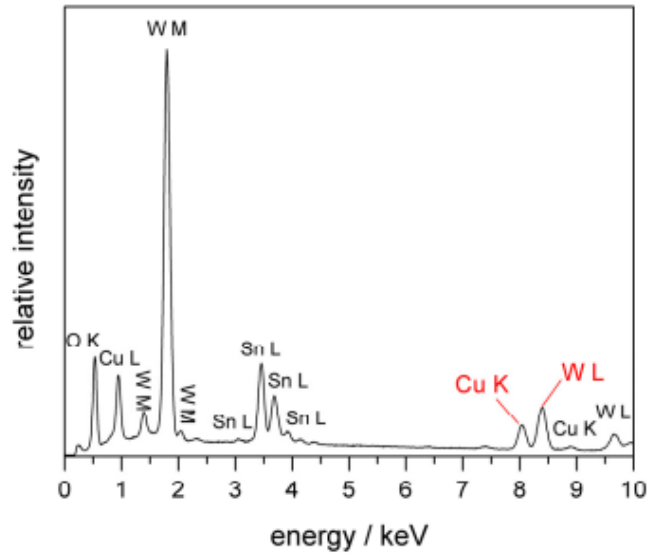


Figure 11: EDX Spectrum of $\text{CuWO}_4\text{-WO}_3$ electrode. The Cu, K, W, and L lines were used for quantifying the W: Cu mole ratio

The relative intensities of the XRD spectrum peaks indicate that the product is predominately CuWO_4 .

In order to characterize the optical properties of the composite electrodes, the UV-vis-NIR spectrophotometer was used to record the reflectance spectrum of the $\text{CuWO}_4\text{-WO}_3$ composite electrodes. As seen in Figure 12, consistent with what has been previously reported by Yourey et al., there is an indirect absorption band edge around 550 nm, corresponding to a band gap value of approximately 2.4 eV as predicted by the Tauc plot shown in the inset

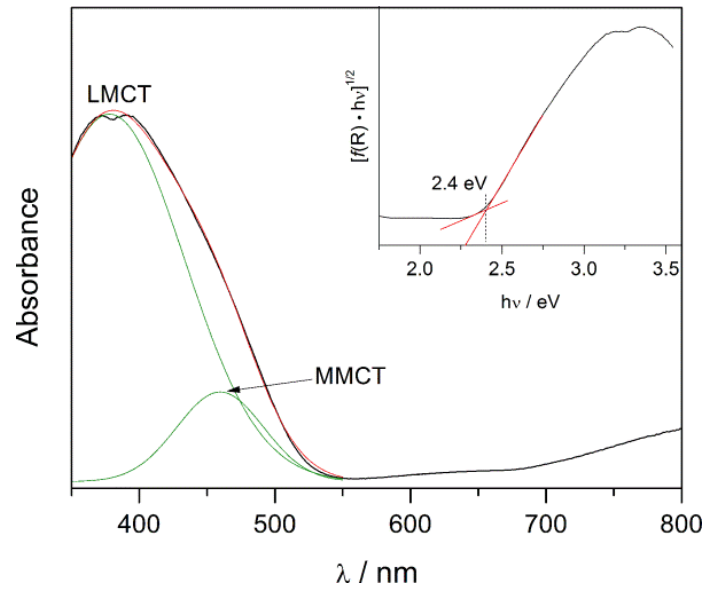


Figure 12: Absorption Spectrum and corresponding Tauc Plot (inset) of $\text{CuWO}_4\text{-WO}_3$ composite electrodes.

Photoelectrochemistry was performed on the $\text{CuWO}_4\text{-WO}_3$ composite electrodes in pH 7 KP_i buffer. At the thermodynamic potential for water oxidation of 0.618 V vs Ag/AgCl or 1.23 V vs RHE, the composite electrodes show an anodic photocurrent of approximately 0.3 mA/cm^2 . Under ambient conditions, bubbling with nitrogen gas, and oxygen gas all of the linear sweep voltammograms show the same onset potential and current profiles as shown in Figure 13. This demonstrates that although the overall ΔE for the reaction is expected to depend on the P_{O_2} according to the Nernst equation, the O_2 has limited water solubility and is removed from the electrode surface faster than it can react.

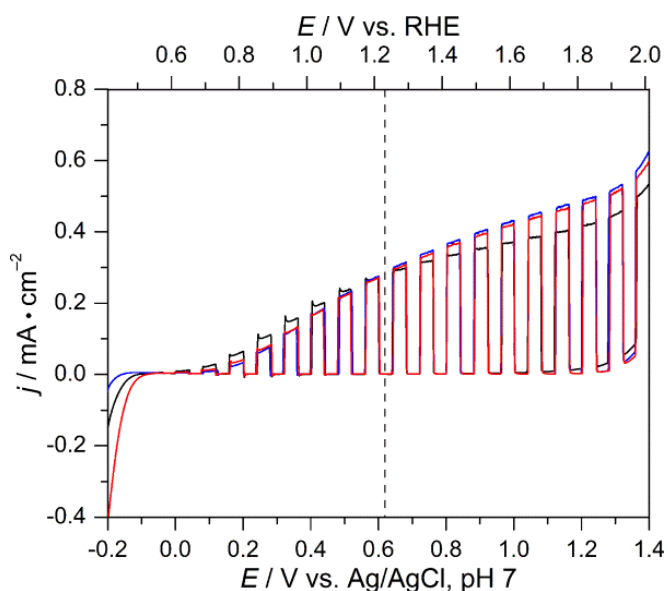


Figure 13: Chopped light linear sweep voltammogram of a $\text{CuWO}_4\text{-WO}_3$ photoanode. Black, red, and blue sweeps are performed in a cell kept under ambient room atmosphere, O_2 , and N_2 respectively.

This photoelectrochemical response was similar for all composite films tested. O_2 data was also collected to confirm the production of oxygen gas from the proposed water oxidation. At an applied bias of 0.5 V vs Ag/AgCl and under 100 mW/cm^2 illumination oxygen was evolved as is shown in Figure 14 on the following page. The theoretical yield of oxygen gas was calculated from the total charge passed at 0.5 V during the experiment. Over the first hour in the dark, but with an applied bias, there is no O_2 gas produced. Once the light is turned on, O_2 evolution begins and the Faradaic efficiency is approximately 85-90% ,which is expected for metal oxides under such conditions.²⁷ Additionally important to note is the fact that a stoichiometric reaction with the approximately 0.5 mg of material deposited on the film surface would only yield approximately 0.16 μmol of oxygen gas. In this case, after 2 hours approximately 1.6 μmol of O_2 are produced, indicating that the $\text{CuWO}_4\text{-WO}_3$ composite is acting as a catalyst in this reaction (i.e. – it is not consumed).

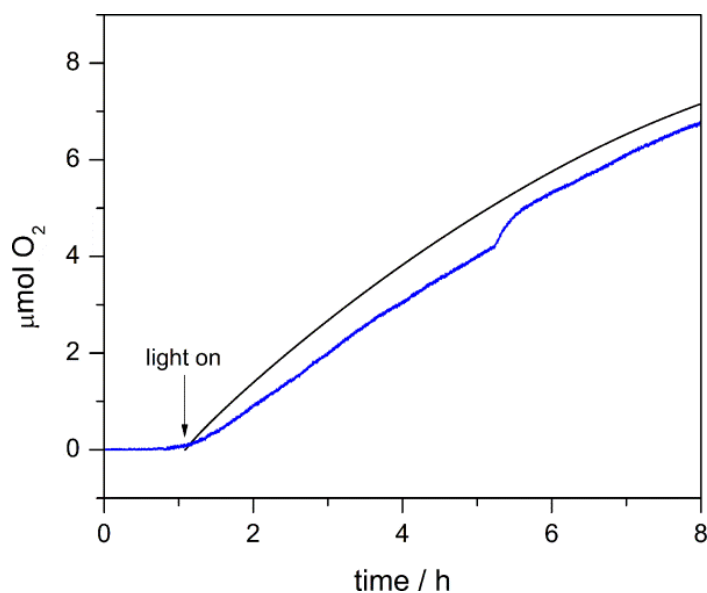


Figure 14: O₂ evolution from an aqueous KP_i solution at +0.5 V (vs Ag/AgCl) using a CuWO₄-WO₃ photocatalyst. Measured O₂ is shown in blue and the theoretical yield based on the total charged passed is shown in black.

These results helped to characterize the photoelectrochemistry of the CuWO₄-WO₃ composite electrodes under aqueous conditions, but as mentioned previously in order to help improve efficiency of the overall water-splitting reaction, a redox mediator can be employed. Towards this end, the two-electrode system was used with 0.1 M KP_i at pH 7 and 100 mM in [Fe(CN)₆]³⁻. Only a two-electrode system may be employed to determine solar-to-hydrogen (STH) efficiency since the potential difference generated by the cathode and anode results from the photogenerated potential. A three-electrode system measures the potential difference between the reference and working electrode and so cannot be used to determine the STH efficiency. The resulting linear sweep voltammogram is shown in Figure 15.

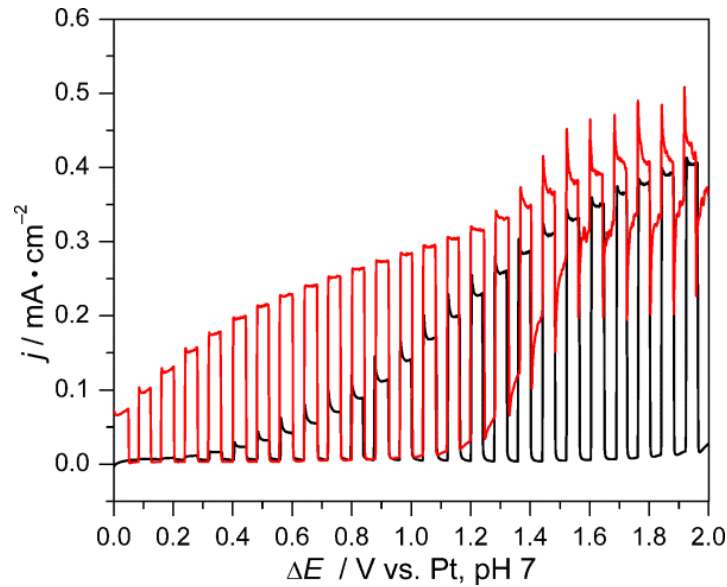


Figure 15: Two-electrode linear sweep voltammogram of aqueous solutions containing 0.1 M KP_i electrolyte (black) and electrolyte plus $100 \mu\text{M } [\text{Fe}(\text{CN})_6]^{3-}$ (red).

Lastly, given that the steady-state current density upon illumination is approximately 0.017 mA/cm^2 , using the equation:

$$H(E_{\text{app}}) = j(E^0 - E^{\text{app}}) / P_{\text{AM1.5G}} \times 100$$

We find that the power conversion efficiency is approximately 0.0065%.

For the films synthesized by sol-gel processing, the UV-Vis spectra collected and the Tauc plot generated from it, report a band gap of approximately 2.45 eV. This bandgap was further estimated by measuring the amount of photocurrent produced as a function of wavelength, with the onset of photocurrent occurring around 530 nm, corresponding to a 2.45 eV energy difference, as can be seen in Figure 16.

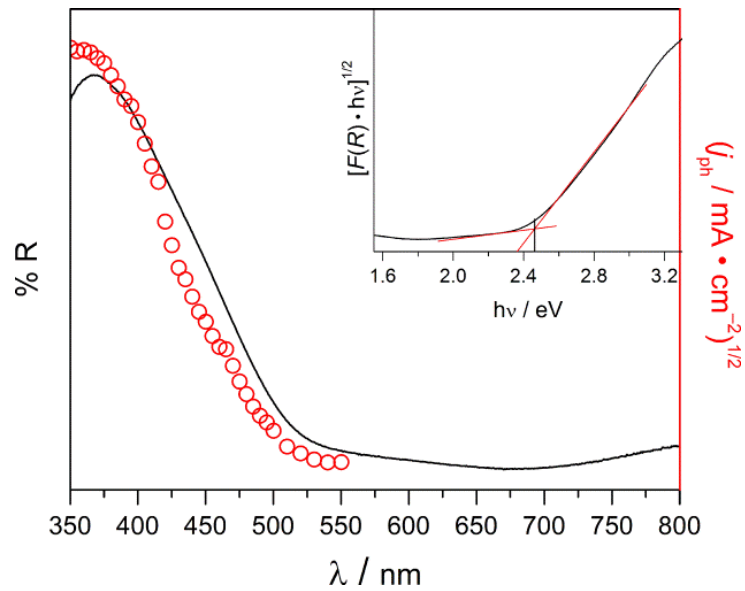


Figure 16: UV-vis diffuse reflectance spectrum (black line) and photoaction spectrum (red circles) of CuWO₄ thin films.

Inset. Indirect band-gap Tauc plot.

The XRD data collected, illustrated in Figure 17, shows that the relative position of the peaks match well with the CuWO₄ powder standard with slightly different intensities and most importantly does not contain distinctive peaks for WO₃, which appear as a small shouldering peak around $2\theta = 24.1^\circ$ and another peak at $2\theta = 33.2^\circ$. EDX analysis further helped to confirm the purity by indicating a Cu:W ratio of 1:1.05, and in corroboration with the ICP-AES data which revealed a Cu:W ratio of 1.06:1. Therefore, we are confident that pure CuWO₄ was synthesized.

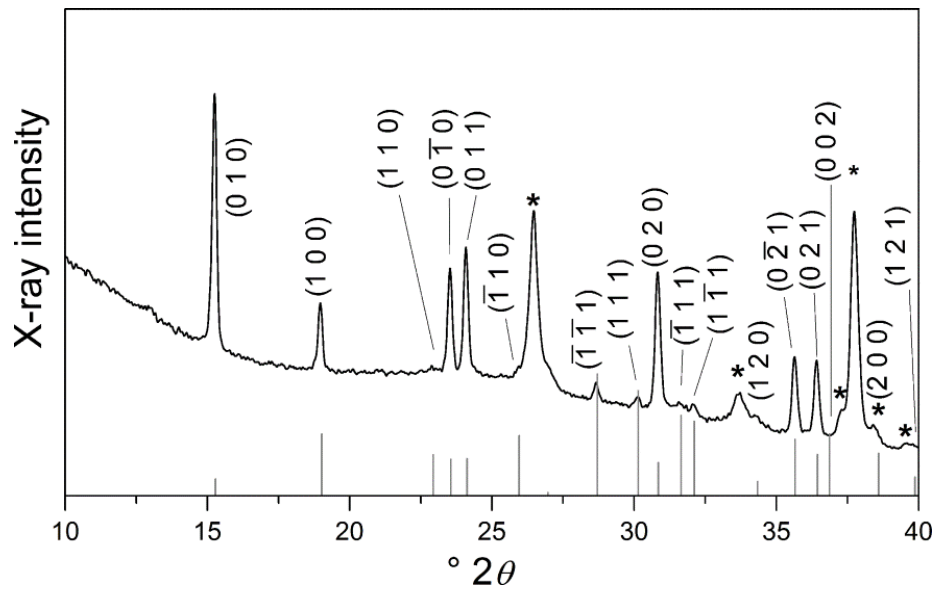


Figure 17: X-ray diffraction pattern of CuWO₄ electrode prepared by sol-gel synthesis.

The photoelectrochemical performance of the pure-phase CuWO₄ films aligns well with the previously reported CuWO₄ prepared by electrodeposition from Yourey et al., as shown in 18 below. The figure shows that the onset of water oxidation in the light occurs at approximately 0.45 V compared to 1.9 V in the dark under 100 mW/cm² illumination. Due to a large overpotential, substantial photocurrent is not observed until approximately 0.7 V vs Ag/AgCl, indicating a substantial kinetic barrier due to substantial charge-transfer resistance.

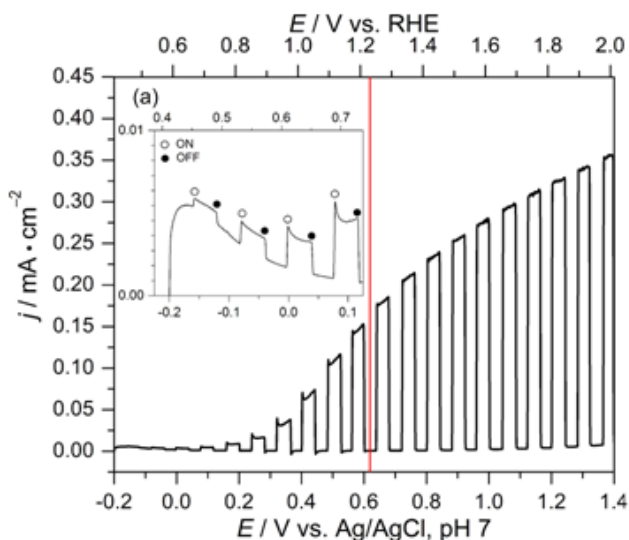


Figure 18: Linear sweep voltammogram, recorded in 0.1 M KP_i buffer at pH 7 and AM1.5G irradiation at $100 \text{ mW}/\text{cm}^2$. **Inset.** Expansion of LSV to illustrate the photocurrent onset potential.

Figure 19 shows the results of the photostability experiments under 1 sun ($100 \text{ mW}/\text{cm}^2$) illumination. CuWO_4 prepared by sol gel synthesis appears to be the most stable under acidic conditions as can be gathered from the smallest decrease in photocurrent (10%) over a four hour period at pH = 3 compared to pH = 5 (12% decrease) and pH = 7 (51% decrease). Despite this substantial decrease in photocurrent at pH=7, it is important to note that the rate of photocurrent decay is significantly less than it is for WO_3 under similar conditions.²⁸ A particularly surprising result came from the comparison of stability under illumination between KB_i and KP_i both at pH=7. In contrast to the significant degradation in photocurrent observed when using pH 7 KP_i buffer (85% decrease over 12 hours), in pH 7 KB_i the photocurrent decreased only 7% over a twelve hour period. This is once again substantially better than the 92% decrease in photocurrent over a 12 hour period for WO_3 . These results indicate that the buffer anion is playing a critical role in the photocurrent decay.

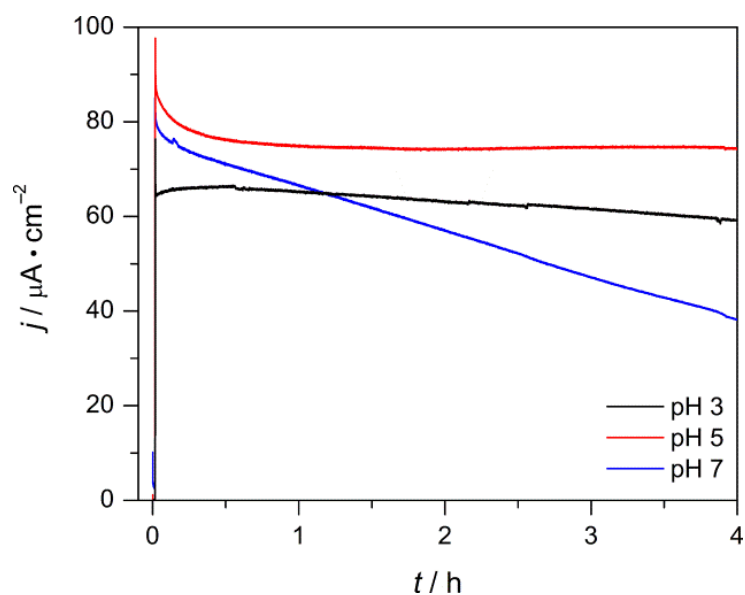


Figure 19: $j-t$ curves of water oxidation on CuWO_4 films in 0.1 M KP_i buffer at 1.23 V vs. RHE under AM1.5G illumination at $100 \text{ mW}/\text{cm}^2$. Black, red, and blue lines represent pH 3, 5, and 7 respectively.

The CuWO_4 electrodes synthesized showed nearly 100% Faradaic efficiency for O_2 production in a solution of equimolar KB_i and NaCl , with $< 2\%$ Cl_2 being detected by a starch-iodine test. Additionally, in order to determine if the presence of accumulated charge on the CuWO_4 electrode surface was leading to degradation, we illuminated the electrode under 3-sun illumination (as opposed to the standard 1-sun that is used for the majority of our experiments). The results in figure 20, show that there are significant transient photocurrents generated with higher power.

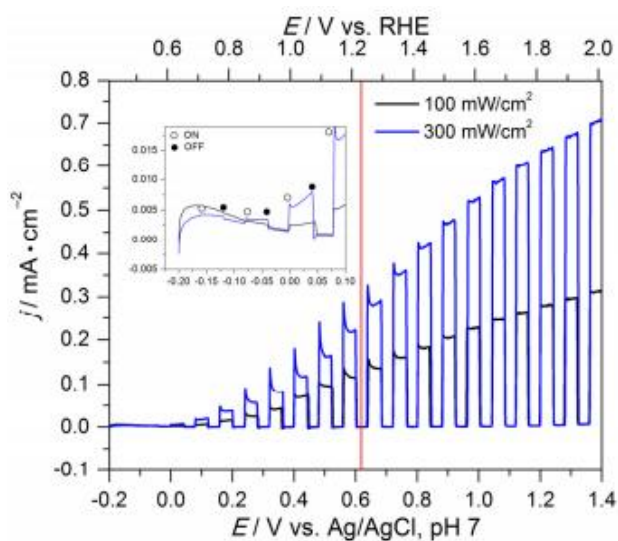


Figure 20: Linear sweep voltammogram of CuWO_4 in 0.1 M KBr with 100 mM NaCl under AM 1.5G 100 mW/cm^2 and 300 mW/cm^2 illumination

For the films prepared by spray pyrolysis, the XRD patterns collected match, as seen in Figure 21, those expected for CuWO_4 , as determined by Jade version 5.0 using the file, JCPDF 72-0616. As in the results for CuWO_4 prepared by sol gel, there are no notable peaks for WO_3 suggesting that electrodes created by spray pyrolysis also generate pure-phase materials. Being able to control the quantity of each Cu and W precursor that is deposited onto the film surface allows for better control of the product formed and helps to prevent the formation of unwanted byproducts due to incorrect ratios.

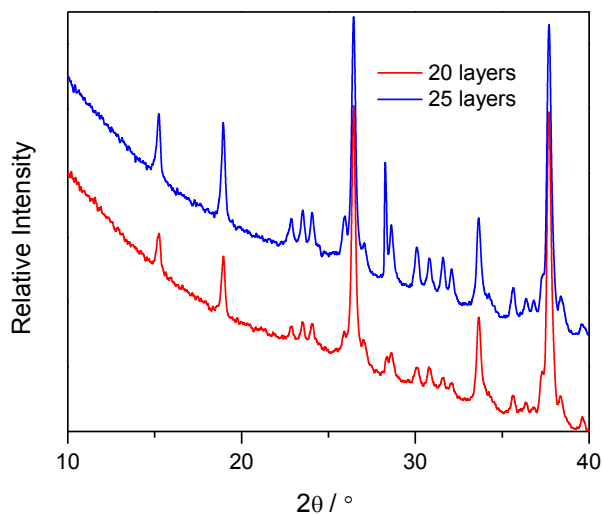


Figure 21: XRD Pattern of CuWO_4 prepared by spray pyrolysis of varying thickness.

Next, we quantify film thickness by recording the absorbance spectrum for electrodes with differing number of sprays on the film surface, shown in Figure 22. As the film thickness increases, we expect that the absorbance should increase because there is more electrode material available for photon absorption. As expected, with increasing numbers sprays the absorbance increases, suggesting that the film thickness is increasing with increasing spray number. A more direct method of measuring film thickness, such as cross-sectional SEM imaging or ellipsometry will be needed in the future to further validate these results.

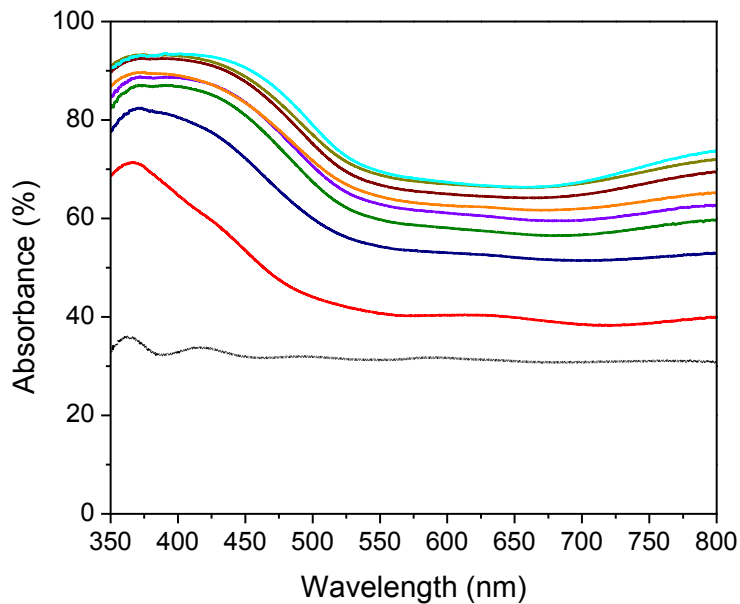


Figure 22: UV-Vis Spectrum of CuWO₄ prepared by spray pyrolysis with varying number of sprays beginning with 10 sprays in red and increasing in increments of 10 to 80 sprays in teal.

In order to determine the film thickness that optimizes overall efficiency, as determined by the overall current passed upon illumination, films with varying numbers of sprays were characterized by

linear sweep voltammetry illustrated in Figure 23. The number of sprays ranged from 10 to 55 and the films were swept from the open circuit to 1.2 V vs. Ag/AgCl in pH 7 KB_i buffer.

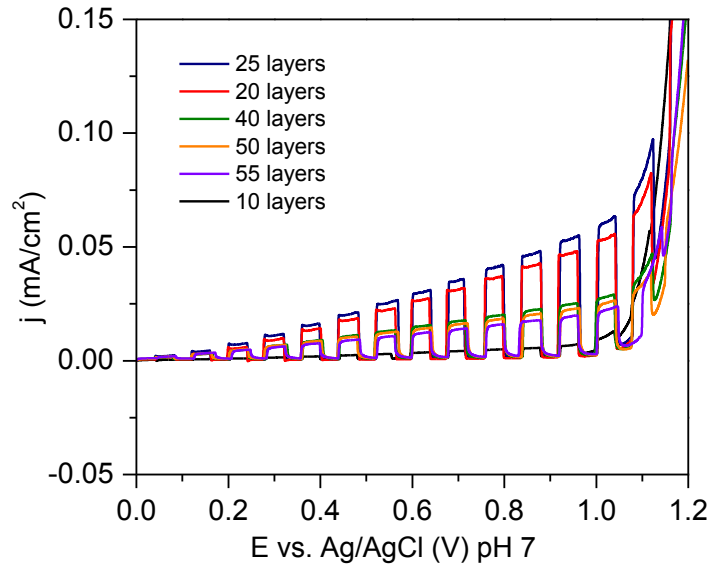


Figure 23: Linear Sweep Voltammogram in 0.1 M KB_i at pH=7 with CuWO_4 prepared by spray pyrolysis with varying numbers of sprays

In order to confirm that the low efficiency with thicker films was the result of electron-hole pairs being generated far from the electrically conductive FTO surface, electrodes were both front and back illuminated and the photocurrent at 0.5 V under 1-sun illumination was measured for electrodes of varying thicknesses, as shown in Figure 24. The rationale for this experiment is that if the electrode is illuminated from the back, electron-hole pairs are generated closer to the conductive surface, giving less time for recombination and increased currents compared to front illumination. This figure shows that as film thickness increases the photocurrent induced from back illumination increases as well with only slight decreases for 60 and 70 sprays, which may result from individual film differences. In contrast, for front illumination, there is a steady increase to about 50 sprays, after which photocurrent begins to decline.

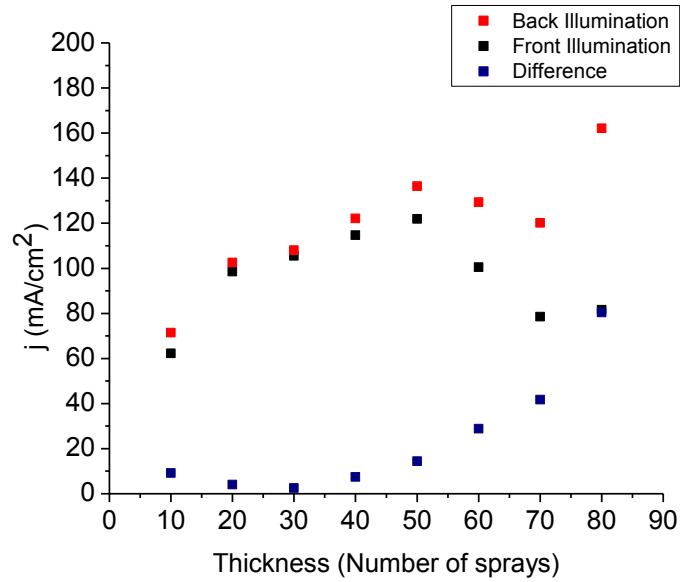


Figure 24: Photocurrent measured under 1-sun illumination and 0.5 V applied bias in 0.1 M KPi at $\text{pH}=7$ for varying film sprays of CuWO_4 .

Perhaps the most interesting result came from the spectral response. In this experiment, the external quantum efficiency (current out per photon in at a given wavelength) is determined at an applied bias of 0.5 V which determines the energy conversion efficiency for water oxidation at the CuWO_4 surface. The plot shown in Figure 25 shows the spectral response measurements as a function of thickness in CuWO_4 films prepared by spray pyrolysis.

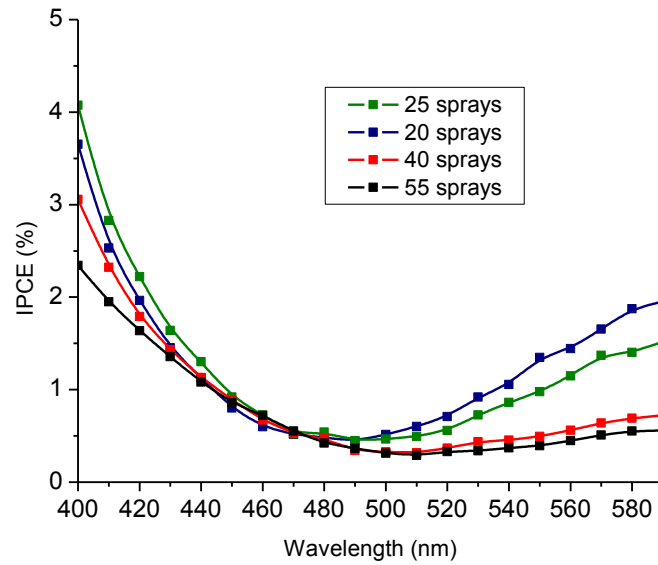


Figure 25: Spectral response of CuWO_4 films prepared by spray pyrolysis with varying thicknesses.

In order to confirm this hypothesis, a film of 25 sprays was illuminated from the front and the back to determine the difference in efficiency. The results of this experiment can be seen in Figure 26 below. While front illumination of the electrode shows a similar increase in spectral response for wavelengths greater than 500 nm, back illumination shows a response that smoothly drops to zero for $\lambda > 500$ nm.

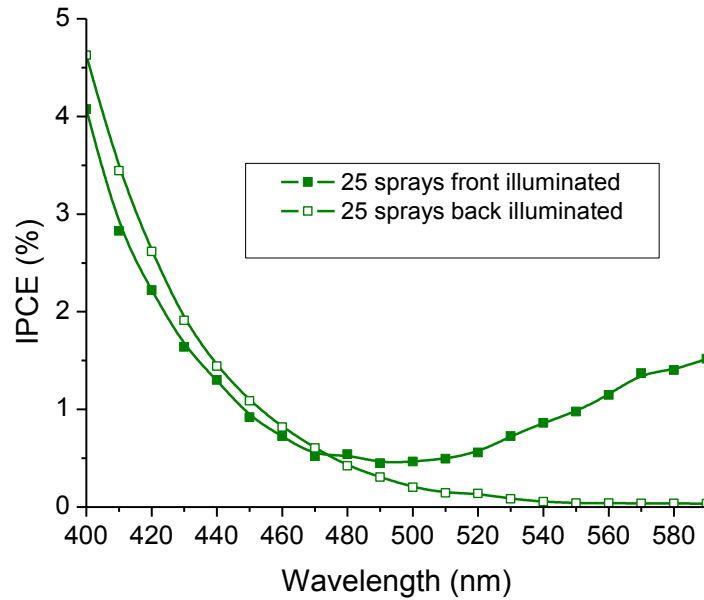
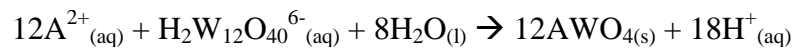


Figure 26: IPCE Spectrum for CuWO_4 films prepared by spray pyrolysis with 25 sprays comparing front and back illumination.

For the solid solution, $\text{Zn}_{1-x}\text{Cu}_x\text{WO}_4$, the XRD data, as shown in Figure 27, indicates that the entire $\text{Zn}_{1-x}\text{Cu}_x\text{WO}_4$ series has been synthesized by the solid state methods described. This data shows a relatively smooth transition between the 2 extremes of CuWO_4 with 4 peaks from $23^\circ 2\theta$ and ZnWO_4 with 2 peaks in this range. Additionally, the peaks corresponding to the (010) and (100) planes are approximately $15.5^\circ 2\theta$ and $19^\circ 2\theta$, respectively. The materials prepared by the Pechini method were synthesized according to the overall reaction scheme:



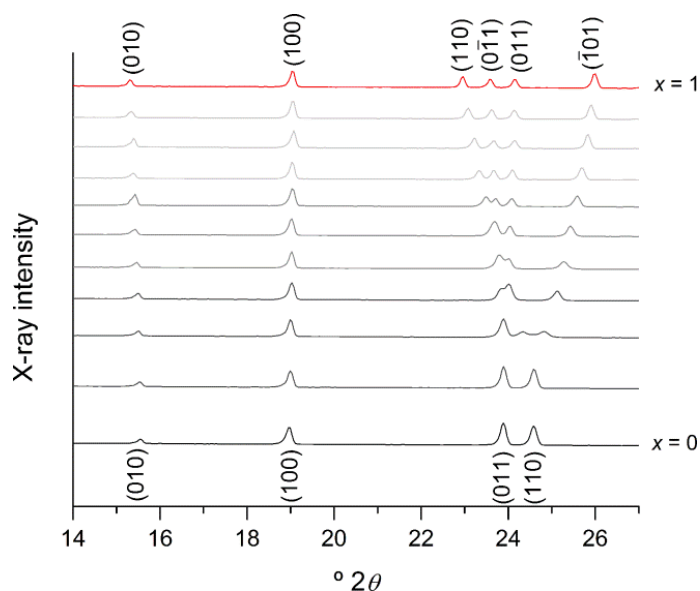


Figure 27: XRD Patterns of $Zn_{1-x}Cu_xWO_4$ series

After a 3 hour annealing step at 700°C , pure phase materials are obtained. Compound purity was confirmed by ICP-AES, which gave the approximate corresponding Cu: Zn ratios expected as can be seen in Figure 28.

x	Cu / mol	Zn / mol	W / mol
0	0	1	0.98
0.1	0.091	0.909	0.99
0.2	0.185	0.815	0.98
0.3	0.279	0.721	1.01
0.4	0.373	0.627	1.01
0.5	0.471	0.529	1.03
0.6	0.572	0.428	1.05
0.7	0.676	0.324	1.05
0.8	0.787	0.213	1.06
0.9	0.896	0.104	1.08
1.0	1	0	1.01

Figure 28: ICP-AES Data for relative mole amounts of Cu, W and Zn in $Zn_{1-x}Cu_xWO_4$ series

The SEM data, shown in figure 29, suggests that the particle sizes are approximately $5\ \mu\text{m}$ for $CuWO_4$ and $1.5\ \mu\text{m}$ for $ZnWO_4$ for the compounds prepared by the solid-state methods, indicating that as the percentage of Cu^{2+} in the compound increases, the particle size increases. This stands in contrast to the

series synthesized by the Pechini method for which there is no change in size for increasing percentages of Cu^{2+} . One possible explanation is that ligand exchange and hydrolysis is much faster for Zn^{2+} , which results in rapid nucleation and smaller particle size.

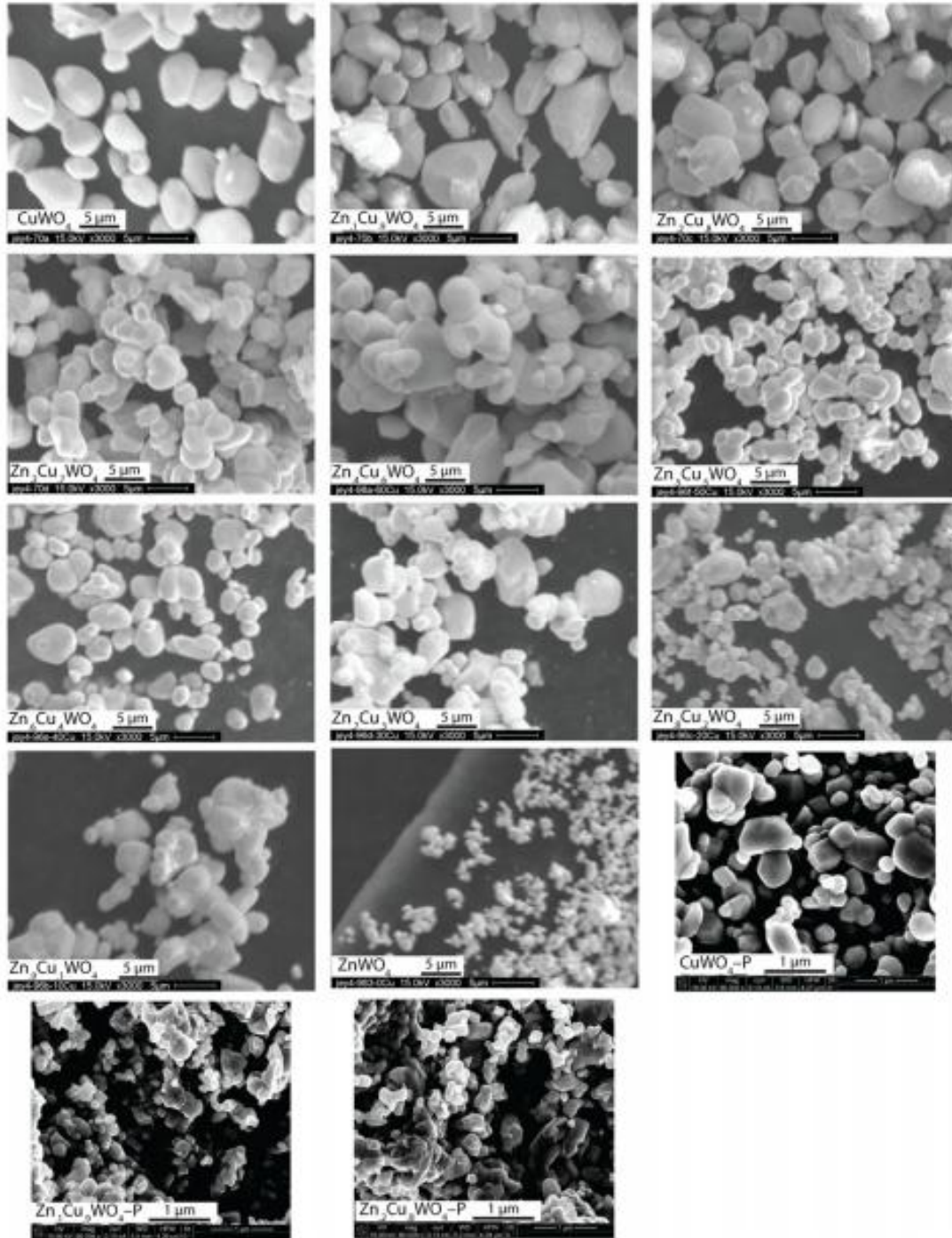


Figure 29: SEM images of $\text{Zn}_{1-x}\text{Cu}_x\text{WO}_4$ ($0 \leq x \leq 1$) by solid state and $\text{Zn}_{1-x}\text{Cu}_x\text{WO}_4$ ($x=0.8, 0.9, 1$) by Pechni sol gel (-P)

Next, band gap measurements were carried out by UV-Vis spectroscopy. To analyze the data more accurately, absorption data were transformed using the Kubelka-Munk function. Both the indirect and direct band gap measurements were recorded for values of $x=0.1$ to 1 in $\text{Zn}_{1-x}\text{Cu}_x\text{WO}_4$. For both the direct and the indirect band gap measurements, there is a decreasing linear trend in band gap as the amount of Cu^{2+} substituted into the lattice increases as shown in figure 30. This suggests that rather than having simply having a mixture of ZnWO_4 and CuWO_4 , the compound formed is of a random mixture of Cu^{2+} and Zn^{2+} ions.

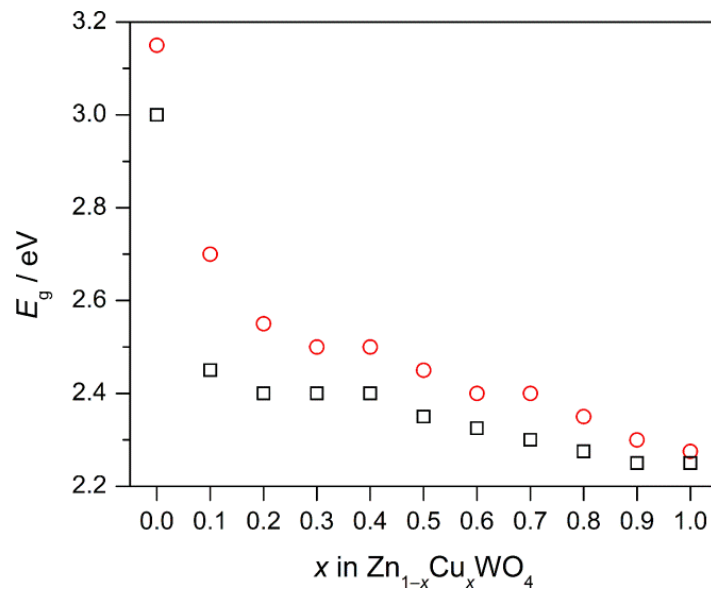


Figure 30: Direct (red circles) and indirect (black squares) band gap energies in the $\text{Zn}_{1-x}\text{Cu}_x\text{WO}_4$ series.

In order to demonstrate that a solid solution was formed as opposed to two separate compounds, the dc magnetic susceptibility data as a function of temperature, $\chi(T)$ recorded at 1 T for the $\text{Zn}_{1-x}\text{Cu}_x\text{WO}_4$ is shown in Figure 31 below.

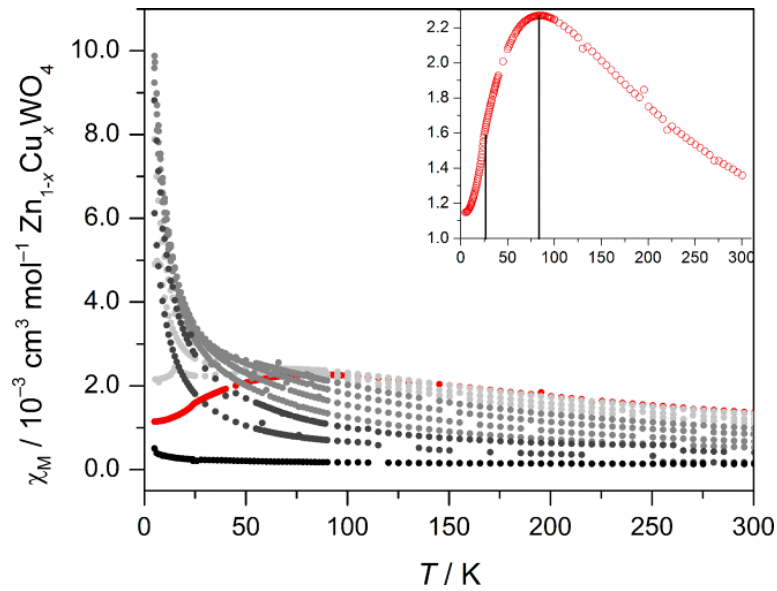


Figure 31: Molar susceptibility of the the $\text{Zn}_{1-x}\text{Cu}_x\text{WO}_4$ series. ZnWO_4 is shown in black, CuWO_4 is shown in red, and intermediate compositions are in gray. **Inset** magnifies the CuWO_4 data and shows two ordering transitions.

For CuWO_4 , the peak maximum occurs at 82 K, and decreases to 69 K for $\text{Cu}_{0.9}\text{Zn}_{0.1}\text{WO}_4$ and further to 59 K for $\text{Cu}_{0.8}\text{Zn}_{0.2}\text{WO}_4$. For compositions with lower than 80% Cu^{2+} , no maximum is observed. In order to determine the Néel temperature (T_N) of CuWO_4 , the first derivative, $d\chi_M/dT$, was taken and maximum was observed at 23.5 K, which matches well with the Néel temperature reported in the literature of 22.5 K, as seen in figure 32.

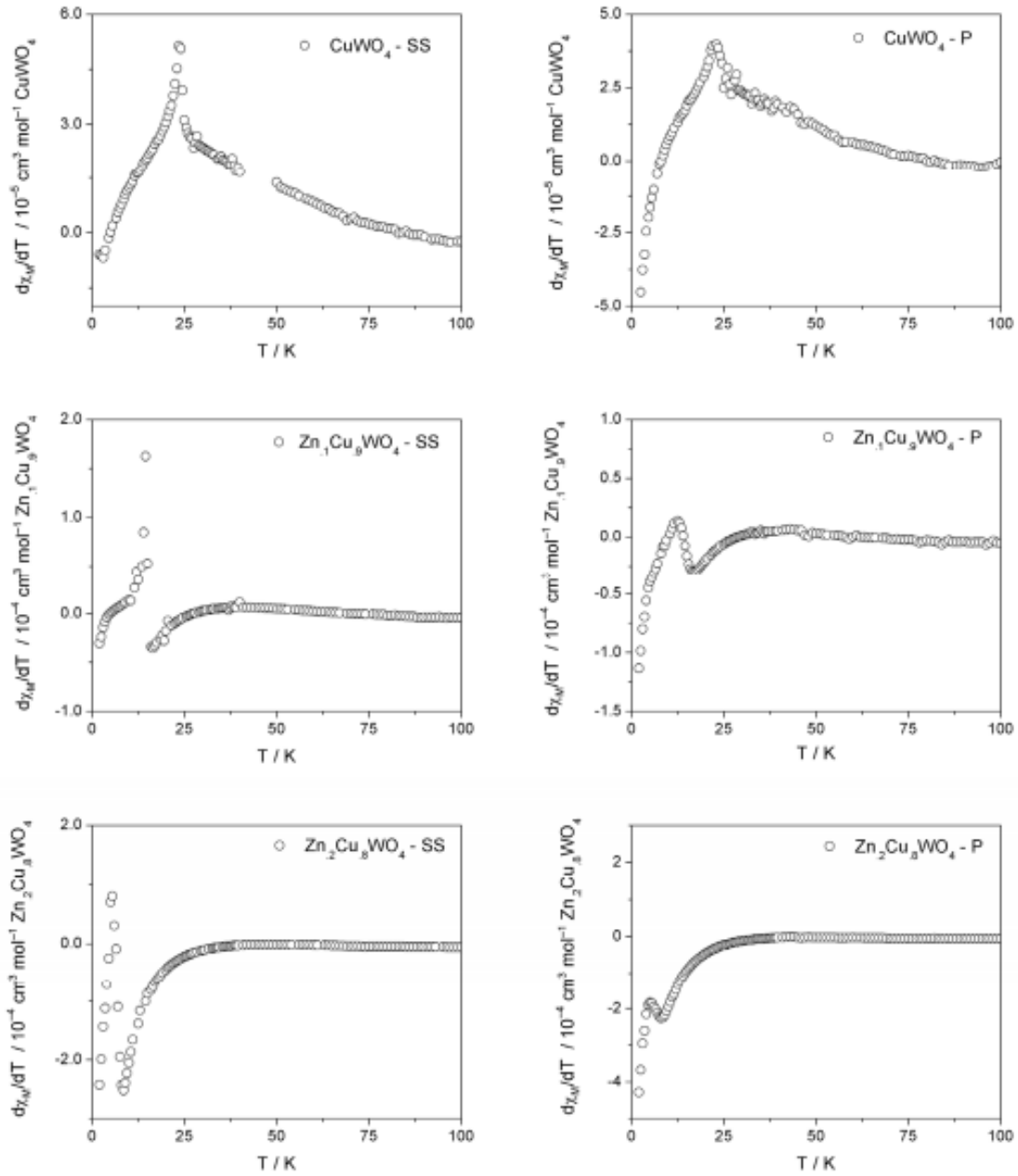


Figure 32: $d\chi/dT$ plots for $\text{Zn}_{1-x}\text{Cu}_x\text{WO}_4$ ($x=0.8, 0.9, 1$) prepared by both solid state (SS) and Pechini sol gel (P)

For $\text{Cu}_{0.9}\text{Zn}_{0.1}\text{WO}_4$ and $\text{Cu}_{0.8}\text{Zn}_{0.2}\text{WO}_4$ T_N was also determined by this method to be 14.5 K and 5.5 K respectively. For these same compounds prepared by the Pechini synthesis, the T_N values were similar.

In order to compare the magnetic susceptibility measurements of the solid solution and the two phase mixtures of compounds, CuWO_4 , a 1:1 mixture of ZnWO_4 : CuWO_4 , and $\text{Zn}_{0.5}\text{Cu}_{0.5}\text{WO}_4$ were all measured. These results are presented in Figure 33. Comparing the shape of the $\chi(T)$ plots for

$\text{Zn}_{0.5}\text{Cu}_{0.5}\text{WO}_4$ and the 1:1 mixture of $\text{ZnWO}_4:\text{CuWO}_4$, we note that they are distinct, indicating that the $\text{Zn}_{0.5}\text{Cu}_{0.5}\text{WO}_4$ mixture is not simply a mixture of the CuWO_4 and ZnWO_4 . Additionally, the 1:1 mixture of $\text{ZnWO}_4:\text{CuWO}_4$ follows the same $\chi(T)$ profile as the CuWO_4 , but with approximately $\frac{1}{2}$ the overall susceptibility as is expected; these comparisons help to verify that a solid solution is formed.

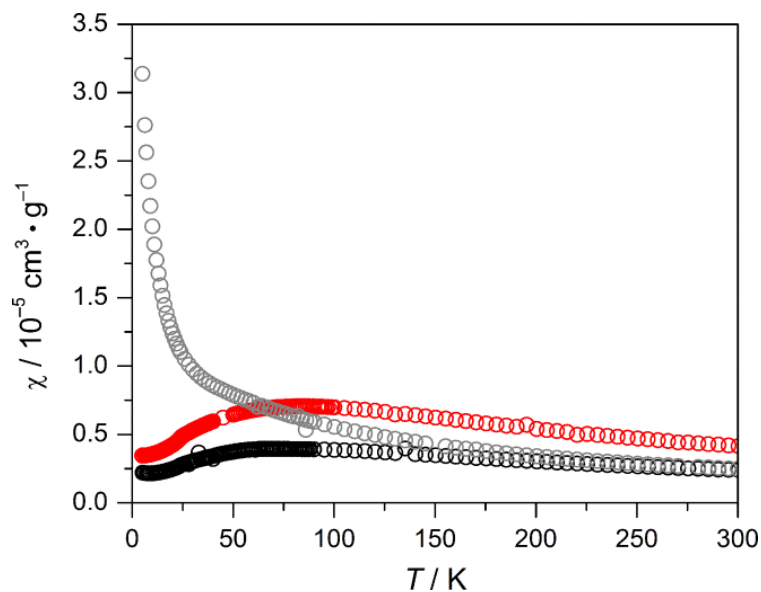


Figure 33: Comparison of the gram susceptibility of CuWO_4 (red), a 1:1 mixture of $\text{ZnWO}_4:\text{CuWO}_4$ (black), and the compound $\text{Zn}_{0.5}\text{Cu}_{0.5}\text{WO}_4$ (gray).

Discussion

Beginning with the $\text{CuWO}_3\text{-WO}_3$ composite electrodes, the onset potential of water oxidation begins at a more negative potential with the addition of $[\text{Fe}(\text{CN})_6]^{3-}$ as should be expected. With no applied bias (i.e. at 0 V), 0.06 mA/cm^2 of photocurrent is observed in $100 \text{ mM } [\text{Fe}(\text{CN})_6]^{3-}$ in contrast to no photocurrent at 0 V without the presence of the sacrificial reductant. In fact, an applied bias of 0.6 V is necessary to generate this same photocurrent in the absence of the redox mediator. Although the overall yield of 0.0065% is very low overall, we note that photosynthesis is typically 3 – 5 % efficient. Given this three order of magnitude difference, there is still need for significant improvement and one possible solution to this problem may be co-catalyst loading with a well-known water oxidation co-catalyst such as cobalt phosphate or NiOOH^{29} , which has shown to increase the efficiency of O_2 evolution in WO_3 films³⁰.

Despite the poor overall conversion efficiency, it is important to note that these results suggest a significant step towards an overall Z-scheme approach to water-splitting using $\text{CuWO}_4\text{-WO}_3$ composite electrodes. Additionally, $\text{CuWO}_4\text{-WO}_3$ electrodes show substantially improved stability under neutral pH conditions as previously reported by Yourey et. al compared to WO_3 electrodes which are generally only stable under highly acidic conditions.

While the $\text{CuWO}_4\text{-WO}_3$ composite electrodes were capable of oxidizing water with only sunlight and no applied bias, the CuWO_4 electrodes prepared by sol gel showed another advantage. The oxidative window of the supporting electrolyte is critical to consider to ensure that it is not preferentially oxidized in place of water. One of the major drawbacks of WO_3 as a photoanode is that it has been shown to preferentially oxidize Cl^- to form Cl_2 in place of performing the desired water oxidation.²³ This is a serious problem considering the fact that significant majority of the earth's water contains sodium chloride, calling into question how practical WO_3 will be as a photoanode on a larger scale. We note that CuWO_4 is that CuWO_4 is selective for water oxidation in the presence of Cl^- , a

distinct advantage of this material compared to WO_3 . A possible explanation is that the valence band of CuWO_4 consists of Cu 3d and O 2p orbitals whereas that of WO_3 consists almost entirely of O 2p. This results in the valence band of CuWO_4 being placed about 0.5 V more positive than that of WO_3 , making Cl^- oxidation substantially less favored for CuWO_4 compared to WO_3 . This is a powerful result as it has strong implications for large-scale hydrogen production, which is likely to be performed using water which contains substantial concentrations of NaCl. This result strongly suggests CuWO_4 is a more selective photoanode for solar-driven water oxidation.

As mentioned previously, for indirect band-gap materials, such as CuWO_4 , light penetrates far into the film. Thus, indirect materials have electron-hole pairs generated closer to the FTO surface and are expected to have increasing amounts of photocurrent with increasing film thickness, but this does not appear to be the case with the CuWO_4 synthesized by sol-gel. It is difficult to determine whether or not this is the result of an inherent flaw with CuWO_4 in that it has a localized 3d conduction band which may inhibit charge transport or if it is the result of the synthetic method which could create unfavorable junctions between layers. Due to the localized 3d character of the conduction band, CuWO_4 is a charge-transfer insulator which necessitates a thin film for high current density. This design unfortunately opposes the need for a thicker material to maximize absorption for the indirect band gap material. A potential drawback of CuWO_4 may be present in the fact that we originally assumed that the conduction band may have been composed of a mixture of Cu 3d and W 5d orbitals, but recent DFT calculations suggest that the conduction band consists primarily of Cu 3d orbitals that reside at potentials more positive than the W 5d orbitals.²⁹ This electronic structure suggests that the Cu 3d orbitals may act as midgap states. To circumvent this structural flaw, a plausible solution involves doping in transition metals to alter the valence band energy, changing its composition to be more homogenous.³¹

The improved stability of CuWO_4 prepared by sol-gel in KB_i compared to KP_i is especially interesting. A possible explanation for the differing stabilities may stem from the relative ratios of the acidic and basic species of each buffer at pH 7. KP_i consists of approximately 61% H_2PO_4^- and 39% HPO_4^{2-} whereas KB_i consists of 99.3% of H_3BO_3 and 0.7% H_2BO_3^- at pH of 7. Perhaps, the anions more selectively interact with the water oxidation intermediates and CuWO_4 than does the neutral boric acid. This also explains the slightly decreased photocurrent with KB_i compared to KP_i . The KP_i buffer is expected to have a better ionic strength than the KB_i which is expected to aid in charge transfer and increase photocurrent.

Another factor that may lead to degradation is the presence of accumulated charge on the CuWO_4 electrode surface. To test this hypothesis, we illuminated a CuWO_4 electrode with 3 sun power (as opposed to the standard 1 sun that is used for the majority of our experiments) and observe transient photocurrents with the higher power. These transients suggest that there is substantial recombination occurring at this power level. This observation hints at the fact that charge may be accumulating on the surface of the CuWO_4 electrodes, which may lead to degradation, although will not be expected to affect the Faradaic efficiency.

For films prepared by spray pyrolysis, electrodes with 10-25 sprays show an increase in photocurrent at any given potential with increasing number of sprays. For thicknesses greater than 25 sprays, there is a decrease in the amount of photocurrent generated. This expected result is the consequence of the competition between photon absorption and useful electron-hole pairs generated as previously mentioned. For films with fewer sprays, although the electron-hole pairs are generated nearer to the FTO substrate decreasing the opportunity for recombination, there is also limited photon absorption because the film is so thin. For thicker films, the opposite is true; although there is a substantial amount of photon absorption, the electron-hole pairs are generated too far from the

electrically conductive surface and so recombination results. The 25 sprays results in an ideal film thickness that optimizes both of these factors.

The difference in photocurrent between back illumination and front illumination shows a steadily increasing trend with increasing film thickness. This result suggests that as the film thickness increases, although the thicker films absorb more light as evidenced by the absorbance spectra, they are unable to transport useful electron-hole pairs to the FTO surface. The difference in back and front illumination increases as a function of film thickness due to increased recombination for films that are front-illuminated.

For the spectral response measurements, as expected we see highest efficiencies (>2%) at wavelengths for which CuWO_4 absorbs optimally (400 - 440 nm). Notable is the slight increase in efficiencies in wavelengths greater than 500 nm, for which CuWO_4 does not absorb particularly well. The longer wavelengths front illuminated light will penetrate further into the film surface generating electron-hole pairs nearer to the FTO conductive surface, leading to less recombination, greater current density, and improved efficiency.

Moving on to the $\text{Zn}_{1-x}\text{Cu}_x\text{WO}_4$ series results, the data suggests that a solid solution of $\text{Zn}_{1-x}\text{Cu}_x\text{WO}_4$ has been formed. Of particular note is the magnetic susceptibility data. For values of Cu^{2+} that are greater than 0.8, there is antiferromagnetic ordering for temperatures greater than T_N . This behavior is not observed in CuWO_4 alone, although the transition is attributed to a strong antiferromagnetic interaction. Rather, this transition as seen in the $\text{Zn}_{1-x}\text{Cu}_x\text{WO}_4$ series for $x \geq 0.8$ mimics the transition seen in CuO , which shows a similar ordering that results from cooperative to noncooperative magnetism, as previously described by Wucher.³² Additionally, for the solid solutions that are more highly substituted with Cu^{2+} , we observe a decrease in the Néel temperature with increasing Cu^{2+} substitution, which matches with previous determinations. Specifically, in MnWO_4 , an

analogous compound, it has been shown that doping in diamagnetic ions such as Zn^{2+} results in a decrease in the Neel temperature.³³

In regards to how these results are specifically useful towards the goal of water oxidation, the highest performing electrodes we have synthesized consist of a composite of CuWO_4 - WO_3 . Studying, the $\text{Zn}_{1-x}\text{Cu}_x\text{WO}_4$ series as a model system for charge transfer barriers and reaction kinetics. Specifically, by incorporating the closed-shell Zn^{2+} ion, the idea was to minimize potential mid-gap states that could increase recombination rates as are present at the junction between the CuWO_4 and WO_3 interfaces. But perhaps of greater interest is the fact that the optical data presented suggests a smooth transition in structure from ZnWO_4 to CuWO_4 , and this suggests that perhaps the band structures of these intermediate structures will follow suit. These materials could combine visible light absorption in CuWO_4 with the favorable more negative conduction band edge in ZnWO_4 . ZnWO_4 has a conduction band edge of -0.4V vs. RHE (compared to $+0.4\text{V}$ for CuWO_4), meaning that ZnWO_4 can liberate H_2 . Balancing the size of the overpotential, as determined by the relative size of the band gap, and the efficiency of photon absorption show potential for increased rates of water oxidation.

Conclusion

Towards the aim of harvesting a renewable energy source, we have focused our attention on CuWO_4 as the photoanode for the water oxidation half reaction and have compared it to the WO_3 model system. CuWO_4 is more chemically stable at $\text{pH} > 5$ than is WO_3 and is selective for water oxidation in saline solution making it a more viable candidate for large-scale hydrogen production. Additionally, we have prepared this material by a variety of methods: electrodeposition, sol-gel processing, and spray pyrolysis.

We were able to generate $\text{CuWO}_4\text{-WO}_3$ composite electrodes by electrodeposition which showed improved performance over the CuWO_4 electrodes. But more importantly, in order to improve the overall efficiency of the water-splitting process, these composite electrodes present a potential Z-scheme approach to water-splitting, whereby the water oxidation and proton reduction reactions are performed by separate electrodes. We have shown that using the redox mediator, $\text{K}_3\text{Fe}(\text{CN})_6$, composite electrodes were able to produce O_2 gas at no applied electrical bias. Overall, this resulted in a conversion efficiency of 0.0065%, which although low compared to current efficiencies in the field, can be potentially improved by the addition of co-catalysts.

Moving away from electrodeposition as a synthetic technique due to the difficulty of controlling W and Cu deposition ratios, we next used a modified sol-gel Pechini synthesis to create pure-phase CuWO_4 electrodes by spin-coating. Of particular interest, was the fact that these electrodes showed improved stability in a neutral KB_i buffer system in contrast to a neutral KP_i buffer system. This result suggests that the buffer anion is playing a significant role in the degradation of the CuWO_4 electrode. The difference in the stability between the two buffers may be the result of the fact that at $\text{pH} 7$, there is very little anionic species present in KB_i in contrast to KP_i . We have also shown that

CuWO₄ electrodes show a significant advantage for water-splitting over the WO₃ counterparts for large-scale hydrogen production – they do not preferentially oxidize Cl⁻ in aqueous solution.

The sol-gel electrodes synthesized allowed for pure-phase CuWO₄ electrodes to be synthesized, but unfortunately resulted in relatively uneven distribution of the material on the film surface despite attempts to circumvent this problem using a Triton-X surfactant. For this reason, we turned our attention towards using spray pyrolysis as a synthetic method, which allows for good control of relative Cu and W ratios and for an even distribution of photoanode material over the FTO surface. We were able to synthesize pure-phase CuWO₄ electrodes as evidenced by XRD, and created a series of films of increasing thickness as shown by increasing absorbance by UV-Vis.

Electrode thickness must be optimized in order to balance photon absorption with proximity of electron-hole pairs generated to the electrically conductive substrate. As shown by linear sweep voltammetry, there is indeed an optimal thickness for CuWO₄ photoanodes, beyond which photocurrent substantially drops leading to poorer overall efficiencies. Additional evidence for this claim is given by an increasing difference between photocurrent observed at 0.5 V with 1-sun illumination for back illumination compared to front illumination as film thickness increases. As film thickness increases electron-hole pairs are generated closer to the CuWO₄ material surface and further from the electrical contact leading to increased recombination and lower photocurrent compared to back illumination of the same electrodes. Additionally, spectral response measurements show greater efficiencies with longer wavelengths for thinner films that are able to generate electron-hole pairs closer to the back contact, decreasing the likelihood of recombination, and increasing photocurrent. When films are illuminated from the back, this increase in responsivity for longer wavelengths disappears due to the electron-hole pairs being generated further from the FTO for longer wavelengths.

Lastly, noting that our highest performing electrodes were 1:1 composites of CuWO₄ and WO₃, we moved towards creating a mixed metal photoanode. Instead of creating two separate phases where

interfaces between the phases may lead to kinetically-limiting barriers, we aimed to synthesize a solid solution of the $\text{Zn}_{1-x}\text{Cu}_x\text{WO}_4$ series. The XRD data shows a smooth transition from ZnWO_4 to CuWO_4 with increasing x . The magnetic susceptibility data shows a transition from antiferromagnetic ordering to paramagnetism at the Néel temperatures for compounds with x values of 0.8 or greater.

Additionally, in contrast to a 1:1 mixture of ZnWO_4 to CuWO_4 , which shows a predominately CuWO_4 -like susceptibility curve, but with half the intensity, the $\text{Zn}_{0.5}\text{Cu}_{0.5}\text{WO}_4$ susceptibility curve is distinct, verifying that a solid solution is formed instead of a two-phase mixture. By using this $\text{Zn}_{1-x}\text{Cu}_x\text{WO}_4$ as a model system for how electron-transfer kinetics are affected in a solid solution compared to a composite system, we can move towards improved water oxidation. And lastly, by balancing the favorably placed conduction band of ZnWO_4 , which is able to perform H^+ reduction and the smaller band gap of CuWO_4 allowing for increased absorption of visible light, solid solutions such as these show promise for future work in electrode optimization.

CuWO_4 electrodes have shown promise in better understanding the role of the supporting electrolyte in electrode stability and towards employing an overall Z-scheme approach to solar driven water-splitting. Looking to the future, CuWO_4 electrodes may be further optimized by controlling film thickness and incorporation of co-catalysts to improve overall efficiencies towards large-scale hydrogen production.

Acknowledgements

Joe Yourey – Throughout my time in the Bartlett lab, Joe was an outstanding graduate student research mentor. He guided me throughout my three years in the Bartlett lab teaching me all I know about research methods, answering any questions I had, and being more than helpful with anything I asked. He has been a wonderful role model and friend and for that I would like to thank him.

Bart Bartlett – Bart has been a wonderful research advisor to work under for the past 3 years. He was always very patient when I asked questions and was very instrumental in helping me to become independent in lab. This push to think independently has driven me to develop a passion for research and for that I would like to thank Bart.

Bartlett Lab Members – The members of the Bartlett lab make every day in lab a joy and are always willing to lend a hand with setting up experiments and answering questions whenever the need arises. They made time in lab so much fun and created a welcome environment and for that I would like to say thank you!

University of Michigan Chemistry Department – The Chemistry Department has provided me with funding for research throughout my undergraduate education without which I may not have been able to afford to stay over the summer to perform research. Additionally, it has provided me many opportunities, including the opportunity to teach as an Undergraduate Instructional Aid, which has helped to shape my future career path for which I would like to say thank you.

Honors Program – The Honors Summer Fellows program supplied funding for my research last summer and provided a wonderful opportunity to meet inspiring researchers from across campus and disciplines. The HSF Cohort taught me a great deal about research methodology and established many meaningful connections and for that I would like to say thank you.

References

- ¹Total energy consumption. (2013, January 1). *Global Energy Statistical Yearbook 2013*. Retrieved from <http://yearbook.enerdata.net/>
- ² N. S. Lewis, D. G. Nocera, *Proc. Natl. Acad. Sci. USA*, 2006, **103**, 15729.
- ³ Kunzig, R. (2013, May 9). Climate Milestone: Earth's CO₂ Level Passes 400 ppm. *National Geographic*. Retrieved , from <http://news.nationalgeographic.com/news/energy/2013/05/130510-earth-co2-milestone-400-ppm/>
- ⁴Intergovernmental Panel on Climate Change (2007) Climate Change 2007, Synthesis Report Summary for Policymakers (Intergovernmental Panel on Climate Change, Washington, DC), Third Assessment Report.
- ⁵J. A. Turner, *Science*, 1999, **1**, 981
- ⁶Lehninger, A., Nelson, D., & Cox, M. (2008). *Principles of Biochemistry*. Chicago: W H Freeman & Co.
- ⁷ Becquerel, E. *C. R. Acad. Sci.* **1839**, 9, 561.
- ⁸ *Nature* **7**, 303 (20 February 1873).
- ⁹A. Fujishima and K. Honda, *Nature*, 1972, 238, 37.
- ¹⁰Gerischer, *J. Electroanal. Chem.*, **1977**, 82, 133-143
- ¹¹ Rohde, R. Greenhouse Effect. (2013, April 20). Retrieved from http://www.globalwarmingart.com/wiki/File:Solar_Spectrum_png
- ¹²Taiz, L., & Zeiger, E. (2010). *Plant Physiology*. : Sinauer Associates, Inc..
- ¹³ J. Desilvestro and M. Gratzel, *J. Electroanal. Chem.*, 1978, 238, 129.
- ¹⁴S. K. Arora, T. Mathew and N. M. Batra, *J. Phys. D: Appl. Phys.*, 1990, 23, 450.
- ¹⁵S. K. Arora, T. Mathew, B. Chudasama and A. Kothari, *J. Cryst. Growth*, 2005, 275, e651.

- ¹⁶Yourey, J. E.; Bartlett, B. M. J. *Mater. Chem.* 2011, 21, 7651.
- ¹⁷Khyzhun et al., *Journal of Alloys and Compounds*, **2009**, 480, 184-189
- ¹⁸Mi, Q.; Zhanaidarova, A.; Brunshwig, B. S.; Gray, H. B.; Lewis, N. S. A Quantitative Assessment of the Competition between Water and Anion Oxidation at WO₃ Photoanodes in Acidic Aqueous Electrolytes. *Energy Environ. Sci.* 2012, 5, 5694–5700.
- ¹⁹Gaillard, N.; Chang, Y.; Braun, A.; DeAngelis, A. Copper Tungstate (CuWO₄)-Based Materials for Photoelectrochemical Hydrogen Production. *Mater. Res. Soc. Symp. Proc.* 2012, 1446, 19–24.
- ²⁰Gaillard, N.; Chang, Y.; DeAngelis, A.; Higgins, S.; Braun, A. A Nanocomposite Photoelectrode Made of 2.2 eV Band Gap Copper Tungstate (CuWO₄) and Multi-Walled Carbon Nanotubes for Solar-Assisted Water Splitting. *Int. J. Hydrogen Energy* 2013, 38, 3166–3176.
- ²¹Zheng, J. Y.; Song, G.; Kim, C. W.; Kang, Y. S. Facile Preparation of p-CuO and p-CuO/n-CuWO₄ Junction Thin Films and their Photoelectrochemical Properties. *Electrochim. Acta* 2012, 69, 340–344.
- ²²Pilli, S. K.; Deutsch, T. G.; Furtak, T. E.; Brown, L.; Turner, J. A.; Herring, A. M. BiVO₄/CuWO₄ Heterojunction Photoanodes for Efficient Solar Driven Water Oxidation. *Phys. Chem. Chem. Phys.* 2013, 15, 3273–3278.
- ²³Mi, Q.; Zhanaidarova, A.; Brunshwig, B. S.; Gray, H. B.; Lewis, N. S. A Quantitative Assessment of the Competition between Water and Anion Oxidation at WO₃ Photoanodes in Acidic Aqueous Electrolytes. *Energy Environ. Sci.* 2012, 5, 5694–5700.
- ²⁴Fu, H.; Lin, J.; Zhang, L.; Zhu, Y. *Appl. Catal., A* 2006, 306, 58.
- ²⁵Galceran, M.; Pujok, M. C.; Aguiló, M.; Díaz, F. J. *Sol-Gel Sci. Technol.* 2007, 42, 79.
- ²⁶Schofield, P. F.; Redfern, S. A. T. *J. Phys.: Condens. Matter* 1992, 4, 375.

- ²⁷ Seabold, J A.; Choi, K. S. *Chem. Mater.* 2011, 23, 1105.
- ²⁸ Hill, J. C.; Choi, K.-S. Effect of Electrolytes on the Selectivity and Stability of n-Type WO₃ Photoelectrodes for Use in Solar Water Oxidation. *J. Phys. Chem. C* 2012, 116, 7612–7620.
- ²⁹ Smith, R. D. L. ; Prevot, M. S. ; Fagan, R. D. ; Zhang, Z. ; Sedach, P. A. ; Siu, M. Kit Jack; Trudel, S. ; Berlinguette, C. P. Photochemical Route For Accessing Amorphous Metal Oxide Materials For Water Oxidation Catalysis. *SCIENCE* **2013**, 340, 60-63.
- ³⁰ Lalić, M. V.; Popović, Z. S.; Vukajlović, F. R. Electronic Structure and Optical Properties of CuWO₄: An ab Initio Study. *Comput. Mater. Sci.* 2012, 63, 163–167.
- ³¹ Palankovski, V.; Kaiblinger-Grujin, G.; Selberherr, S. Study of dopant dependent band gap narrowing in semiconductor devices. *Materials Science and Engineering.* 1999, 46-49.
- ³² Wucher, J. *Acad. Sci. Paris* 1955, 241, 288.
- ³³ Obermayer, H. A.; Dachs, H.; Schröcke, H. *Solid State Commun.* 1973, 12, 779.